PLOS Genetics

RESEARCH ARTICLE

A novel peptidoglycan deacetylase modulates daughter cell separation in *E. coli*

Víctor M. Hernández-Rocamora[1], Alessandra M. Martorana[2], Aitana Belloso[3], Daniel Ballesteros[3], Marta Zaccaria[2], Amilcar J. Perez[4], Bogdan I. Iorga[5], David Abia[3], Joe Gray[1], Eefjan Breukink[6], Jie Xiao[4], Manuel Pazos[3,7]*, Alessandra Polissi[2]*, Waldemar Vollmer[1,8]*

1 Centre for Bacterial Cell Biology, Biosciences Institute, Newcastle University, Newcastle upon Tyne, United Kingdom, **2** Department of Pharmacological and Biomolecular Sciences "Rodolfo Paoletti", University of Milano, Milano, Italy, **3** Centro de Biología Molecular Severo Ochoa (CBM), CSIC – Universidad Autónoma de Madrid, Madrid, Spain, **4** Department of Biophysics & Biophysical Chemistry, The Johns Hopkins University School of Medicine, Baltimore, Maryland, United States of America, **5** Université Paris-Saclay, CNRS, Institut de Chimie des Substances Naturelles, Gif-sur-Yvette, France, **6** Membrane Biochemistry and Biophysics, Bijvoet Centre for Biomolecular Research, Department of Chemistry, Utrecht University, Utrecht, The Netherlands, **7** Instituto Universitario de Biología Molecular (IUBM) y Departamento de Biología Molecular, Universidad Autónoma de Madrid, Madrid, Spain, **8** Institute for Molecular Bioscience, The University of Queensland, Brisbane, Queensland, Australia

* mpazos@cbm.csic.es (MP); alessandra.polissi@unimi.it (AP); w.vollmer@imb.uq.edu.au (WV)

OPEN ACCESS

Citation: Hernández-Rocamora VM, Martorana AM, Belloso A, Ballesteros D, Zaccaria M, Perez AJ, et al. (2025) A novel peptidoglycan deacetylase modulates daughter cell separation in *E. coli*. PLoS Genet 21(9): e1011626. https://doi.org/10.1371/journal.pgen.1011626

Editor: Aretha Fiebig, Michigan State University, UNITED STATES OF AMERICA

Received: February 14, 2025

Accepted: August 25, 2025

Published: September 5, 2025

Data availability statement: All raw data are presented in the manuscript.

Funding: This work received funding from the UK Biotechnology and Biological Sciences Research Council (BB/W005557/1; BB/

Abstract

Peptidoglycan hydrolases facilitate bacterial cell wall growth by creating space for insertion of new material and allowing physical separation of daughter cells. In *Escherichia coli*, three peptidoglycan amidases, AmiA, AmiB and AmiC, cleave septal peptidoglycan during cell division. The LytM-domain proteins EnvC, NlpD and ActS activate these amidases either from inside the cell or the outer membrane: EnvC binds to the cytoplasmic membrane-anchored divisome components FtsEX, while NlpD and ActS are outer membrane-anchored lipoproteins. Here we report the identification of a novel periplasmic deacetylase called SddA that removes acetyl groups from denuded peptidoglycan glycan strands, the products of amidases. The *sddA* gene is co-expressed with the gene encoding EnvC, linking SddA function to amidase activation. Consistent with this link, the deletion of *sddA* alleviates phenotypes associated with lack of amidase activation, while overexpression of *sddA* alleviates phenotypes related to a defective Tol-Pal system and causes cell chaining due to reduced septum peptidoglycan cleavage. We present a model according to which SddA modulates the activation of the septum-splitting amidases during cell division.

Author summary

Bacteria surround their cell membrane by the essential peptidoglycan (cell wall) layer to prevent bursting open due to their turgor. During cell division, bacteria

W013630/1; to W.V.), from the National Institutes of Health (NIH R35 GM136436 to J.X. and NIH F32 GM150262 to A.J.P.), from MICIU/AEI/https://doi.org/10.13039/501100011033 and ERDF/EU (PID2022-140818OA-I00; to M.P.), the Comunidad de Madrid Atracción de Talento M1 program (2020-T1/BMD-19970, to M.P.). A.B. acknowledges a PhD fellowship from Fundación Ramón Areces. D.B. acknowledges a PhD fellowship (PRE2022-101502) associated to the "Centre of Excellence Severo Ochoa" grant to the CBM (CEX2021-001154-S) funded by MICIU/AEI /https://doi.org/10.13039/501100011033. CBM receives institutional grants from Fundación Ramón Areces. B.I.I. is supported by a grant from the French National Research Agency (ANR) through the PPR Antibioresistance program (ANR-20-PAMR-0010). The funders had no role in study design, data collection and analysis, decision to publish, or preparation of the manuscript.

Competing interests: The authors have declared that no competing interests exist.

produce a septum at midcell, which must be cleaved for daughter cells to separate. Here, we report the identification of a new enzyme, SddA, that modifies a particular type of peptidoglycan material, denuded glycan chains released during the splitting of septal peptidoglycan for daughter cell separation, in the Gram-negative *Escherichia coli*. We propose a model in which SddA modulates a switch in the septal peptidoglycan splitting, ensuring splitting is activated from the cell membrane in the early stages of cell division and from the outer membrane in the late stages.

Introduction

The bacterial peptidoglycan (PG) sacculus provides support against the turgor and maintains the shape of the cell [1]. PG is made of chains of alternating *N*-acetylglucosamine (Glc*N*Ac) and *N*-acetylmuramic acid (Mur*N*Ac) residues with short peptides linked to Mur*N*Ac. Peptides from adjacent strands can be connected by crosslinks to form the PG network surrounding the cytoplasmic membrane [1]. Rod-shaped bacteria such as *E. coli* use membrane-spanning multiprotein complexes for sacculus growth: the divisome facilitates cell division at midcell and the elongasome side wall expansion [2,3]. Both complexes coordinate the activities of various PG-synthesising and hydrolysing enzymes and PG biogenesis is coordinated with outer membrane (OM) synthesis and maintenance [2,4,5].

Cell division is a key process in the cell cycle in which PG synthesis and hydrolysis are coupled. The cytoplasmic tubulin homologue FtsZ forms treadmilling FtsZ polymers rotating around the division site [6–8], attached to the cytoplasmic membrane (CM) by FtsA and ZipA [9]. Early in cell division, PG synthesis is initiated by class A Penicillin-binding proteins (PBPs) [10,11], and it is regulated by SPOR-domain PG-binding proteins such as FtsN [11,12]. Assembly of the complete divisome activates the major cell division-specific synthases FtsW-PBP3 [3]. PG synthases polymerize glycan strands from the PG precursor lipid II and cross-link the peptides [13]. PG hydrolases are needed for splitting the septal PG for the separation of the daughter cells. PG *N*-acetylmuramoyl-L-alanine amidases (amidases) remove the stem peptides from the glycan strands producing 'denuded' strands. In *E. coli*, AmiA, AmiB and AmiC are the major septum-splitting enzymes responsible for daughter cell separation [14,15]. They are periplasmic enzymes with structurally-related catalytic domains and regulated by LytM-domain-containing activators [16]. EnvC activates AmiA and AmiB and is itself activated by the cytoplasmic membrane-anchored FtsEX proteins, which are members of the divisome [17–20]. By contrast, the lipoproteins NlpD and ActS activate AmiC from the OM [21–23]. The regulation of the NlpD/AmiC complex is poorly understood and might involve the Tol-Pal system, but not the OM-anchored lipoprotein DolP, which is crucial for OM integrity and pathogenicity in many γ- and β-proteobacteria [24]. The transmembrane Tol-Pal system facilitates OM constriction during cell division and regulates, via the accessory protein CpoB, the activation of the transpeptidase (TPase) of the PG synthase PBP1B [4]. Knockout of

either the amidases or their regulators, or members of the Tol-Pal system, produces chaining and OM-defects in *E. coli* [14,16,25].

Many bacteria modify the chemical structure of peptidoglycan to adapt to different growth conditions or to resist attacks by hydrolases released by the host or bacteriophages [1,26]. One important modification is the deacetylation of the sugars in the glycan chain, which helps bacteria to resist the digestion of PG by lysozyme. The first PG *N*-acetylglucosamine deacetylase, PgdA, was identified in *Streptococcus pneumoniae* [27], where it contributes to virulence [28], and homologues are present in other Gram-positive bacteria, for example *Listeria monocytogenes* [29] or *Streptococcus suis* [30]. The PgdA catalytic domain contains a NodB-homology domain (PFAM PF01522) with a conserved triad of two histidine and one aspartic residue coordinating Zn^{2+} as metal cofactor [31]. PG deacetylases have been thought to be absent in Gram-negative bacteria. The 'atypical' PG deacetylase suggested to be present in a Gram-negative bacterium, PgdA from *Helicobacter pylori* [32,33], seems to lack a signal peptide for export into the periplasm, and deacetylated PG fragments were not observed in *H. pylori* [34–37]. Interestingly, a recent high-resolution mass spectrometry-based approach identified a small amount (0.25 ± 0.03%) of deacetylated PG glycan fragments (Glc*N*-Mur*N*Ac, S1B Fig) in *E. coli* [38], although *E. coli* does not appear to have a homologue of PgdA and deacetylated disaccharide peptides (muropeptides) were not released from *E. coli* PG by a muramidase [39,40].

In this work, we report the discovery of a new enzyme in *E. coli* that can deacetylate denuded PG glycan strands produced by amidases. The deacetylase, which we named SddA (Septal denuded strand deacetylase A), is genetically linked to the amidase activator EnvC and localizes to the cell division septum. SddA is distantly related to PgdA structurally as both contain catalytic domains belonging to the glycoside hydrolase/deacetylase, beta/alpha-barrel superfamily (Interpro IPR011330). Our results suggest that SddA is involved in regulating amidase activity during cell division by affecting the activation of amidases from the OM or CM.

Results

SddA is a denuded glycan strand deacetylase

We searched the *E. coli* genome for genes encoding for periplasmic proteins with homology to PG deacetylases. A fold-based search using *S. pneumoniae* PgdA as query and the *E. coli* proteome as target yielded 8 hits, of which three are proteins targeted for periplasmic export (PgaB, YadE and YibQ). These proteins contain a polysaccharide domain similar to that of PgdA. PgaB is an OM protein that deacetylates the extracellular poly-β-(1,6)-Glc*N*Ac (PGA) matrix for biofilm formation [41,42]. YadE is a protein of unknown function with genetic links to genes involved in lipid A modification and synthesis [43]. We also identified YibQ, a protein containing a divergent polysaccharide deacetylase domain (protein family PF04748) that is related to but distinct to the deacetylase domain of PgdA (PF01522). Interestingly, the *yibQ* gene locates within the same operon as the PG hydrolase activator gene, *envC* (Fig 1A), and YibQ has a predicted signal peptide for export into the periplasm, making it a candidate for a PG deacetylase. To identify how conserved this genetic linkage is, we determined the distribution of genes encoding for YibQ homologues within the Annotree database which contains a representative set of consistently annotated bacterial genomes [44]. Genes encoding for YibQ homologues are present mainly within genomes of Gram-negative bacteria (Fig 1B), and most of these, including *E. coli yibQ*, are located on the same strand of the DNA (Fig 1C) and within two kilobases to genes encoding for EnvC homologues (Fig 1D). An AlphaFold model of YibQ predicts an N-terminal globular domain with conserved metal binding residues followed by a long C-terminal disordered region (Figs 1E and S2B).

To test if YibQ is the enzyme responsible for the presence of Glc*N*-Mur*N*Ac in *E. coli* PG, we purified PG from *E. coli* BW25113 and an isogenic *yibQ* deletion strain, digested it with the lytic transglycosylase MltA, which is known to be able to digest denuded glycan strands [45] to generate the 1,6-anhydro-disaccharide subunits and analysed these by liquid-chromatography-mass spectrometry (LC-MS/MS) for the presence of Glc*N*-Mur*N*AcAnh and Glc*N*Ac-Mur*N*AcAnh

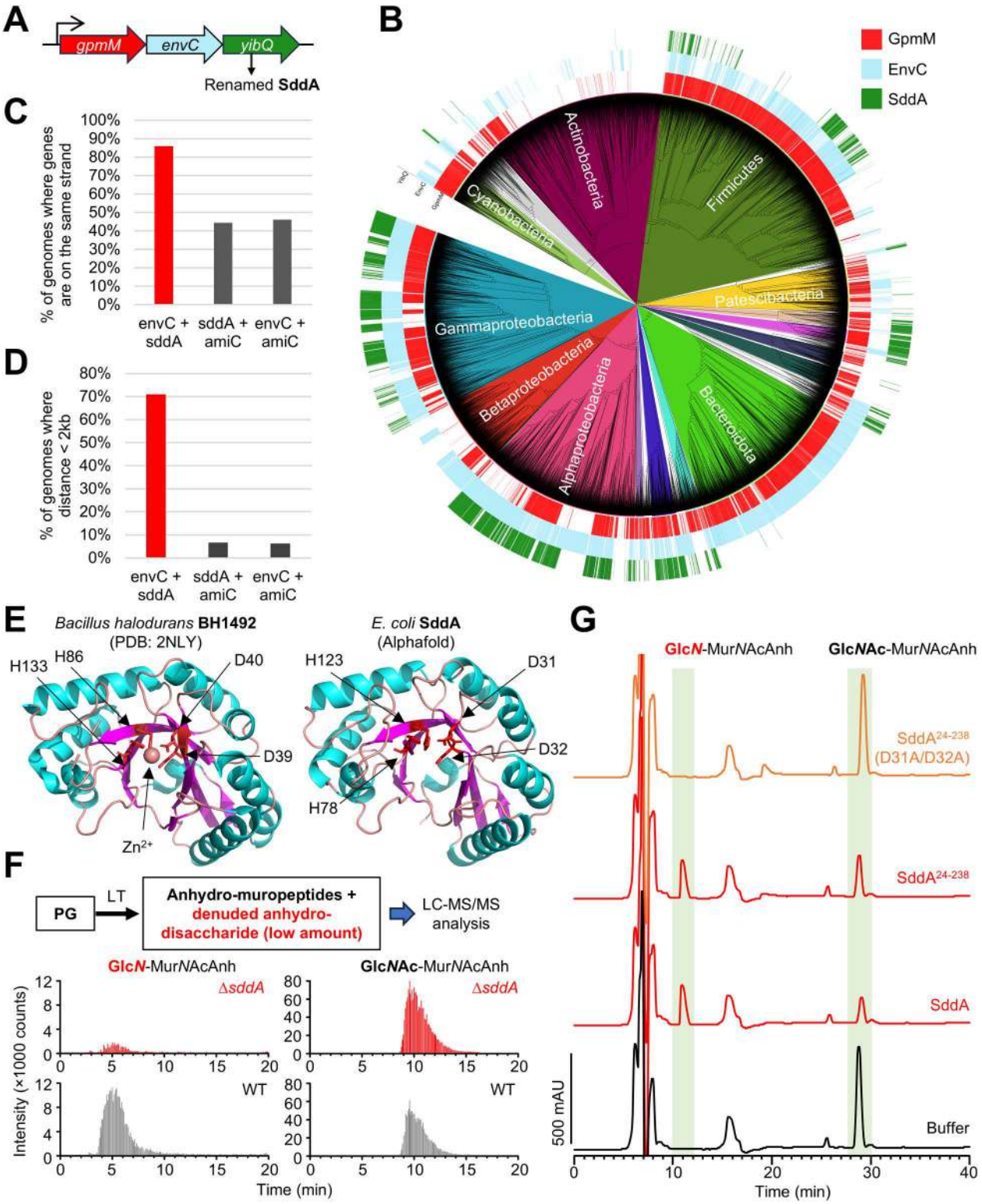

Fig 1. SddA is a denuded PG glycan strand deacetylase genetically linked to amidase activator EnvC. (A) The *E. coli* gene *yibQ* (*sddA*) is located downstream in the same operon as amidase activator *envC*. (B) Distribution of *gpmM*, *envC* and *sddA* homologues in the bacterial genome database Annotree. (C) When *sddA* and *envC* are present in the same genome in Annotree, they are most often present on the same strand. (D) When *sddA* and *envC* are present in the same genome in Annotree they are found most often at a distance of less than 2 kilobases. (E) Alphafold model of the SddA

globular domain (left), compared with the crystal structure of BH1492 from *Bacillus halodurans* (PDB 2NLY), which also contains a divergent deacetylase domain. The residues involved in Zn^{2+} coordination in the BH1492 structure and their homologues in SddA are indicated. (F) Analysis by LC/MS of the presence of Glc*N*-Mur*N*AcAnh and Glc*N*Ac-Mur*N*AcAnh in PG from *E. coli* BW25113 (WT) or *E. coli* BW25113Δ*sddA* (Δ*sddA*), released by MltA. Top, scheme of the procedure, bottom, chromatograms showing intensity of peaks eluting with m/z 437 and 479 corresponding to Glc*N*-Mur*N*AcAnh and Glc*N*Ac-Mur*N*AcAnh, respectively, for WT and Δ*sddA*. The identity of Glc*N*-Mur*N*AcAnh and Glc*N*Ac-Mur*N*AcAnh MS peaks was verified by MS/MS fragmentation (S1 Fig). In the scheme, LT stands for lytic transglycosylase. (G) Chromatograms of the analysis of denuded glycan strands treated first with buffer, SddA, $SddA^{24-238}$ or $SddA^{24-238}$ D31A/D32A, and then with the lytic transglycosylase MltA to produce anhydro-muropeptides. Labelled peaks were identified by mass spectrometry (see text) and correspond to Glc*N*-Mur*N*AcAnh (Glc*N*) and Glc*N*Ac-Mur*N*AcAnh (Glc*N*Ac).

https://doi.org/10.1371/journal.pgen.1011626.g001

(Figs 1F and S1AB). Glc*N*-Mur*N*AcAnh was present in BW25113 and absent in BW25113 Δ*yibQ* (Fig 1F), suggesting that YibQ is responsible for deacetylating Glc*N*Ac residues in denuded strands. Based on these results and results shown below, we renamed YibQ to SddA (Septal Denuded strand Deacetylase A).

SddA is a Glc*N*Ac deacetylase specific for denuded strands

Next, we wanted to determine whether the N-terminally oligohistidine-tagged version of SddA lacking the signal peptide has PG deacetylase activity. However, upon His-SddA overexpression, most of the produced protein was insoluble and the soluble cell fraction contained only a truncated version (S2 Fig). We purified the soluble, truncated His-SddA and used mass spectroscopy to identify the truncation sites by determining the molecular weights of the protein variants present in these preparations. This analysis showed that the truncation happened within the C-terminal flexible region and the protein still contained the whole globular catalytic domain (S2A Fig). To work with a more homogeneous preparation of SddA, we also expressed and purified a truncated version lacking the predicted C-terminal flexible domain entirely, named His-$SddA^{24-238}$, which was completely soluble when overexpressed.

We next tested the activity of His-SddA against whole PG sacculi or muropeptides, which were obtained by digesting PG with a muramidase. No visible changes in the muropeptide profiles were observed in the presence of the His-SddA (S3 Fig), indicating that SddA is not active against PG or muropeptides. Considering the location of *sddA* next to *envC*, we next tested if His-SddA is active against denuded glycan strands. For this, we developed an assay in which radiolabelled, un-crosslinked PG strands were generated with a TPase-defective PBP1B variant and [^{14}C]GlcNAc-labelled lipid II. These strands were then treated with the amidase AmiC in the presence of its activator NlpD to produce radiolabelled denuded glycan strands (S4A Fig). Incubation of these strands with His-SddA prevented their digestion with the muramidase cellosyl (S4B Fig). If the radiolabelled denuded glycan strands were (partially) pre-digested with cellosyl into short glycan strands, His-SddA produced new peaks with different elution times, indicating that SddA modified denuded glycan strands (S4C Fig). To determine the exact reaction performed by SddA, we prepared denuded glycan strands by complete digestion of purified PG with the amidase AmiD and incubated them with His-SddA. The product was digested with lytic transglycosylase MltA, which is able to completely digest denuded glycan strands [46], and analysed the products by HPLC and mass spectrometry (Fig 1G and S1CD Fig). Treatment of denuded strands with His-SddA produced a decrease in Glc*N*Ac-Mur*N*AcAnh (neutral mass 478.10 amu) and yielded a new peak, identified as Glc*N*-Mur*N*AcAnh (neutral mass 436.05 amu) with MS/MS analysis confirming that deacetylation affects Glc*N*Ac and not Mur*N*Ac (Figs 1G, S1CD). His-$SddA^{24-238}$ generated the same product, confirming that the flexible C-terminal region in SddA is not required for activity. Finally, His-SddA was also able to deacetylate short Glc*N*Ac-Mur*N*Ac oligomers produced by partial digestion of denuded strands by cellosyl (S5 Fig). Overall, these results demonstrate that His-SddA deacetylates GlcNAc residues in denuded strands.

Conserved Asp residues in SddA are required for activity

The Protein Data Bank (PDB) includes two structures of a PF04748 domain, i.e., the same family as the catalytic domain in SddA. In one of these, corresponding to BH1492 from *Bacillus halodurans*, a Zn^{2+} ion is coordinated by two Asp and two

His residues (Fig 1E). These four residues are conserved in SddA: D31, D32, H78, H123 (S6A Fig). To test if these residues are important for SddA activity, we purified SddA versions in which these residues were replaced by Ala and assayed their activity against denuded glycan strands (Figs 1B and S6B). SddA versions D31A/D32A, H78A or H123A showed no activity in this assay (Fig 1G), suggesting that the four conserved hypothetical metal (Zn^{2+})-binding residues are important for SddA activity.

The localization of FtsN SPOR domain is not affected by *sddA* deletion

SPOR domains recognize PG denuded glycan strands allowing proteins bearing these domains to locate to division sites where these strands are produced by amidases [47,48]. These domains are present in the *E. coli* proteins FtsN, DedD, DamX and RlpA. All of these except RlpA have been shown to interact with or activate PG synthases during cell division, and they contain a single transmembrane helix anchoring them to the cytoplasmic membrane (Fig 2A) [12,47,49,50]. We

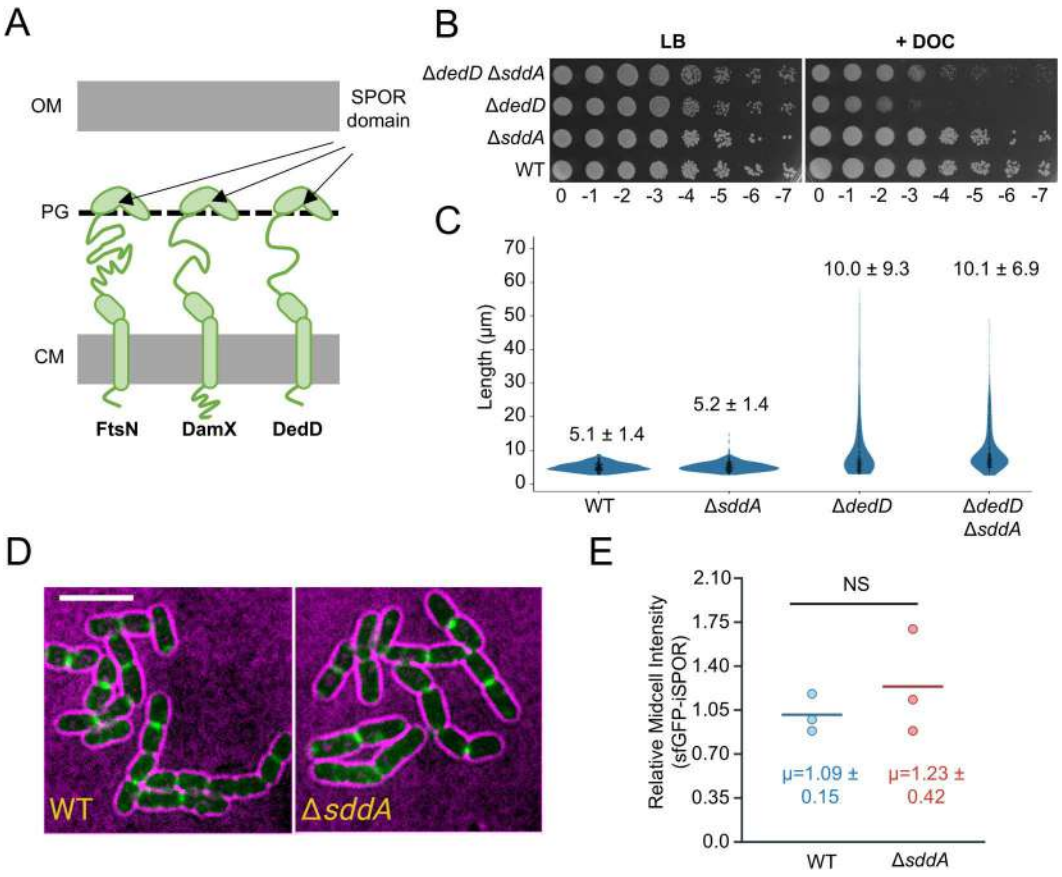

Fig 2. Effect of *sddA* deletion on SPOR domain proteins. (A) Scheme showing the three SPOR domain proteins anchored to the cytoplasmic membrane (CM) of *E. coli,* which bind denuded glycan strands at midcell and participate in cell division regulation. (B) Ten-fold serial dilutions spotted plate of BW25113 (WT), MP005 (Δ*sddA*), MP001 (Δ*dedD*) and MP006 (Δ*dedD* Δ*sddA*) strain cultures incubated at 30°C in LB-Lennox with or without 0.2% (w/v) sodium deoxycholate (DOC). (C) Violin plot showing cell length of the strains in (B), grown at 30°C in LB-Lennox in exponential phase. The mean ± standard deviation (SD) is indicated (n > 300). (D) Representative images of BW25113 (WT) or BW25113 Δ*sddA* (Δ*sddA*) bearing pCH-ss^{dsbA}-sfGFP-iSPOR showing the localization of sfGFP-iSPOR (green) in cells (black cells with magenta background). Scale bar is 5 μm. (E) Quantification of average midcell intensity of sfGFP-iSPOR. Each data point is representative of the mean average value of 29-52 cells "relative midcell intensities" (normalized by the WT median per replicate, see methods). Written is the mean ± SD from three independent biological replicates. NS means not significant (nonparametric Mann-Whitney test).

https://doi.org/10.1371/journal.pgen.1011626.g002

wondered whether the deacetylation of denuded glycan strands could affect the binding of SPOR domain proteins, thus preventing their midcell localization or function. We first asked if the deletion of *sddA* has an effect in a Δ*dedD* background. Cells lacking *dedD* are more elongated and more sensitive to outer membrane (OM) stressors such as detergents [51]. A Δ*dedD* Δ*sddA* strain showed a reduced sensitivity to deoxycholate compared to Δ*dedD* but was still more sensitive than the WT (Fig 2B). In addition, Δ*dedD* Δ*sddA* cells had similar length as Δ*dedD* (Fig 2C), indicating that the deficient cell division phenotype was not restored by *sddA* deletion.

To directly probe SPOR protein recruitment in the absence of SddA, we used fluorescence microscopy to localize the isolated SPOR domain of FtsN tagged with a fluorescent protein (sfGFP-iSPOR) in BW25113 or the isogenic strain lacking *sddA* (Fig 2D). The deacetylation of denuded glycan strands might alter the affinity of SPOR domains and, hence, their recruitment to midcell could be different in the absence of SddA. However, we did not observe a significant difference in midcell localization intensity of sfGFP-iSPOR between the WT and Δ*sddA* strains (Fig 2E), suggesting that either SPOR domains are not affected by deacetylation by SddA or that the activity of SddA at midcell is too low to affect SPOR localization. This result suggests SddA is not involved in the regulation of FtsN localization at midcell. Further studies are needed to explore whether SddA affects the localization and function of DedD, DamX, or RlpA.

SddA function is linked to peptidoglycan amidases

In order to understand the role of SddA in the cell, we investigated phenotypes caused by deleting the *sddA* gene in *E. coli* BW25113. BW25113 Δ*sddA* grew with normal rate and morphology under standard laboratory conditions (S7 Fig), and the lack of *sddA* did not affect OM permeability of mutants lacking one or more amidase activators (S8 Fig). Mutants lacking amidases or amidase activators form chains and become sensitive to detergents such as deoxycholate [52]. We confirmed this phenotype in mutants that depend on either EnvC (Δ*nlpD* Δ*actS*) or NlpD (Δ*envC* Δ*actS*) (Fig 3) for amidase activation. Interestingly, deleting *sddA* in these backgrounds rendered cells less sensitive to deoxycholate, suggesting that removal of SddA enhances amidase activity (Fig 3B). In contrast to the strains depending solely on NlpD or EnvC for amidase activation, the deletion of *sddA* from the strain depending solely on ActS (Δ*envC* Δ*nlpD*) produced a considerable increase in lag phase, although growth rates during exponential phase were similar (S9 Fig). Both, Δ*envC* Δ*nlpD* and Δ*envC* Δ*nlpD* Δ*sddA* produced very long and sometimes twisted cell chains (S9 Fig). Overall, these results suggest that SddA may inhibit PG amidases in some genetic backgrounds. This modulation might be through direct interaction with the amidases and/or their activators, or indirectly through the deacetylated PG product of SddA.

SddA expression from a plasmid causes cell chaining and OM defects

As the deletion of *sddA* in a WT background caused no obvious growth phenotype, we tested the effects of SddA overexpression by inserting the full length *sddA* sequence, including its signal peptide, into an expression plasmid under control of IPTG-inducible *Ptac* promoter yielding pGS100-*sddA*. Addition of IPTG to BW25113 bearing pGS100-*sddA* but not the empty plasmid (pGS100) increased the sensitivity to vancomycin and SDS/EDTA (Fig 4A) and induced the formation of long cell chains (Fig 4B), phenocopying the deletion of amidases or their activators [52] and suggesting that PG amidases are impaired upon SddA overexpression. As *sddA* and *envC* are co-expressed in the same operon on the genome, we tested whether co-expression of both from a single, plasmid-borne operon has the same effects as the expression of the individual proteins. Co-expression of both *envC* and *sddA* from the same operon in a single pGS100-derived plasmid (Fig 4B) produced no cell chaining in BW25113. When *sddA* and *envC* were expressed from separate plasmids (pGS100 and pBAD24, respectively), cell chaining still occurred (S10 Fig). Similarly, co-expression of *nlpD* (from pGS100) and *sddA* (pBAD24) did not suppress either the sensitivity to vancomycin or SDS/EDTA, or cell chaining (S11 Fig). Asking why the presence of *envC* in the same operon with *sddA* abolished *sddA* overexpression phenotypes, we determined the level of FLAG-tagged SddA in BW25113 harbouring a pGS100-derived plasmid encoding FLAG-SddA or EnvC/FLAG-SddA. First, we verified that the expression of FLAG-SddA reproduced the phenotypes of the expression of non-tagged SddA (S12A

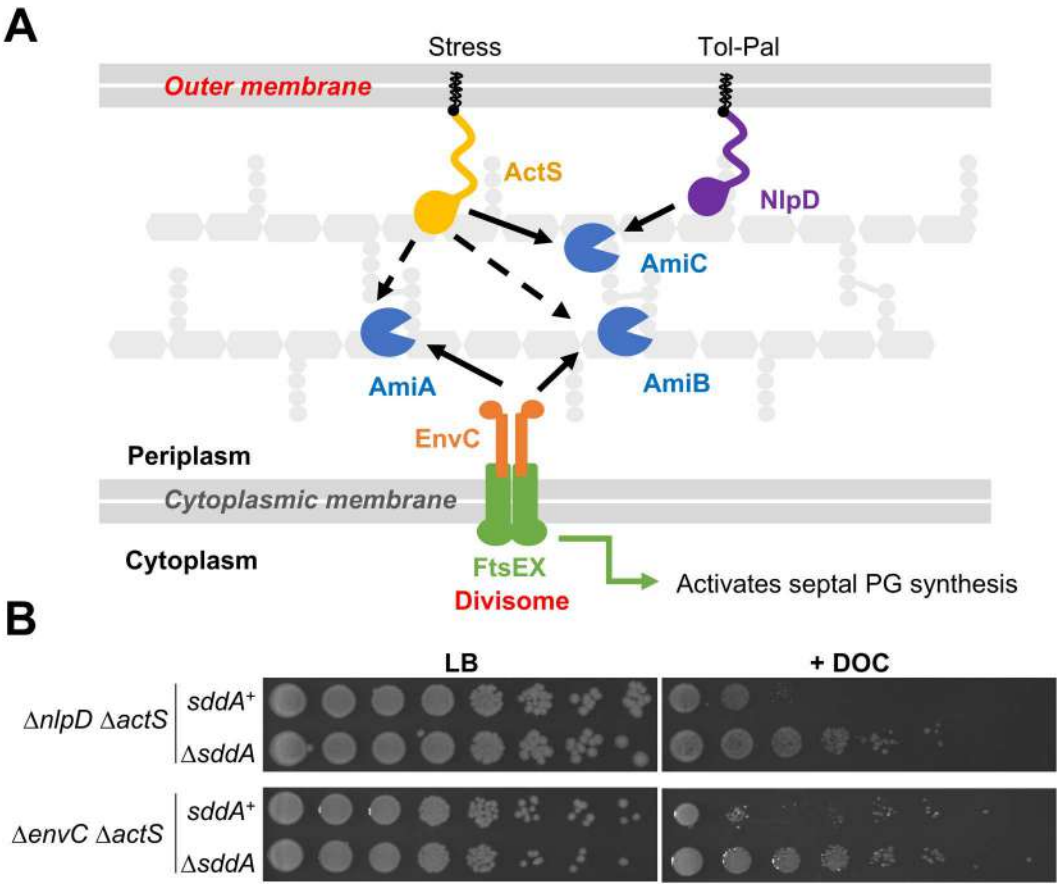

Fig 3. SddA deletion alters deoxycholate sensitivity of strains defective in multiple amidase activators. (A) Scheme depicting amidase activation in *E. coli*. AmiA and AmiB are activated by the FtsEX-EnvC complex, which is part of the divisome, from inside the cell. AmiC is activated by lipoproteins NlpD and ActS. ActS can also activate AmiA and AmiB *in vitro* (dashed arrows). (B) Ten-fold serial dilutions spotted plates of BW25113 Δ*nlpD* Δ*actS* and BW25113 Δ*nlpD* Δ*actS* Δ*sddA* (top), and BW25113 Δ*envC* Δ*actS*, and BW25113 Δ*envC* Δ*actS* Δ*ssdA* (bottom). Plates were incubated at 37°C. Top plates contain LB with or without 0.5% deoxycholate (DOC). Bottom plates contain LB-Lennox with or without 0.5% deoxycholate (DOC).

https://doi.org/10.1371/journal.pgen.1011626.g003

Fig). Next, we quantified the production of FLAG-SddA upon induction with IPTG by Western blot (S12B Fig). Interestingly, in addition to full-length FLAG-SddA, a lower molecular band was also detected, indicating that the C-terminus of SddA can be digested in the cell (S12B Fig). Levels of FLAG-SddA were ~3 times lower when FLAG-SddA was expressed in an operon with *envC* (S12B Fig), suggesting that the lack of chaining upon FLAG-SddA expression from this plasmid could be due to a lower expression level. Overall, these results suggest that the chaining caused by SddA depend on its expression levels, which is controlled by co-expression with *envC*.

Consistent with the above results, deletion of *envC* or *ftsX* did not rescue the cell chaining caused by SddA overexpression (S13 Fig). Moreover, overexpression of SddA in cells lacking *envC* and its cognate amidases (*amiA* and *amiB*), or *nlpD* and its cognate amidase (*amiC*), aggravated the cell chaining phenotype (S14 Fig). These results indicate that neither amidase system (EnvC-AmiA/B or NlpD-AmiC) is functional upon overexpression of SddA. In addition, the overproduction of SddA in Δ*envC* Δ*amiA* Δ*amiB* cells produced a sicker phenotype than overproduction of SddA in Δ*nlpD* Δ*amiC* as judged by an extensive cell chaining and highly defective growth phenotype (S14 Fig). Noteworthy, Δ*envC* Δ*amiA* Δ*amiB* cells are already sicker than Δ*nlpD* Δ*amiC* cells in the controls with the empty plasmid (S14 Fig).

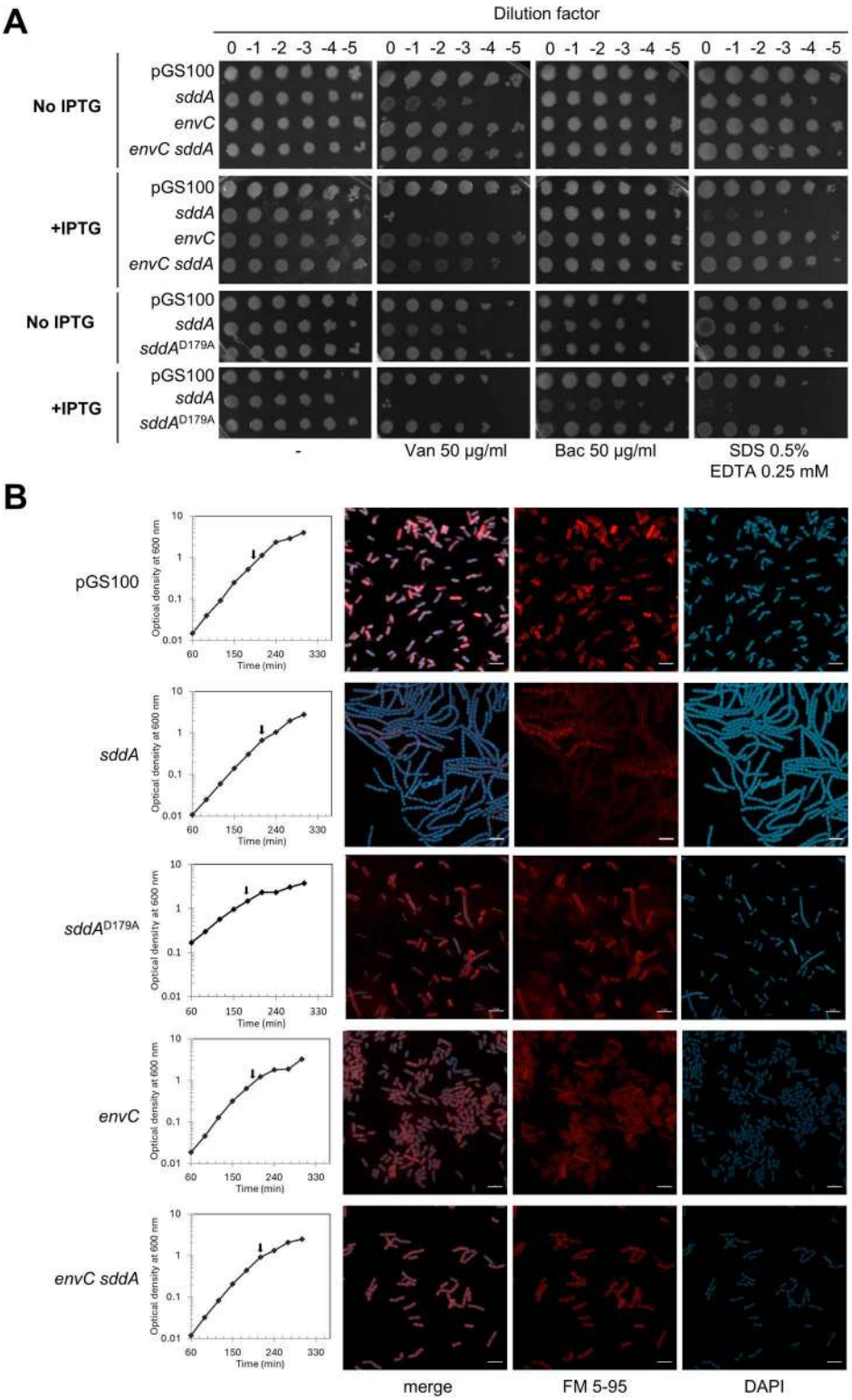

Fig 4. High SddA levels cause OM defects and cell chaining unless *envC* is overexpressed. (A) Overnight cultures of BW25113 harbouring pGS100 or pGS100 expressing *sddA, sddA*^{D179A}, *envC or* both *envC* and *sddA* were serially diluted and spotted onto LB-Lennox supplemented with 25 µg ml^{-1} chloramphenicol and antibiotics or chemicals at the indicated concentrations, with or without 0.5 mM IPTG. Plates were incubated at 37°C for

24 h. (B) BW25113 cells harbouring pGS100 or pGS100 expressing *sddA, sddA*^{D179A}*, envC* or both *envC* and *sddA* were grown in LB-Lennox supplemented with 25 μg ml^{-1} chloramphenicol and 0.5 mM IPTG. Samples were collected at exponential phase (arrows), stained with FM5-95 (red, cell membrane) and DAPI (blue, nucleoid), immobilized and imaged by confocal fluorescence microscopy. Representative images are shown. Scale bar is 5 μm.

https://doi.org/10.1371/journal.pgen.1011626.g004

Finally, we tested whether the activity of SddA is required to inhibit PG amidases by studying the effects of overproduction of FLAG-tagged SddA H123A, which is inactive (S6B Fig). FLAG-SddA H123A levels in BW25113 expressed from pGS100 were similar to those of FLAG-SddA (S12B Fig). However, expression of this inactive version did not cause cell chaining (S12A Fig), suggesting that SddA activity is required to regulate cell separation.

In summary, these results suggest that high levels of enzymatically active SddA inhibit cell separation, and this effect does not depend on the presence of one specific amidase or amidase regulator.

SddA localizes at cell division sites

The cell chaining phenotype caused by expressing SddA from a plasmid suggests that SddA can reduce the activation or activity of amidases at midcell, preventing daughter cell separation. If this inhibition relies on a direct interaction with septal amidases or their activators, SddA should localize at midcell. To determine the cellular localization, we expressed an SddA-sfGFP fusion containing the native SddA signal peptide from pGS100. Western blot analysis of cell extracts showed no cleavage of the fluorescent tag, indicating that the SddA-sfGFP fusion is stable (S15A Fig). Expression of SddA-sfGFP resulted in cell chaining, similar to the expression of the unlabelled protein, and these effects depended on the amount of IPTG added to cells (S15B Fig). Interestingly, the fluorescence signal localised to the uncleaved septa in cells expressing SddA-sfGFP (Fig 5A). When induction level was lower (25 μM IPTG), SddA-sfGFP did not cause cell chaining and still localized at midcell in dividing cells (Fig 5AB). Next, we examined the effect of aztreonam on SddA localization. Aztreonam is a β-lactam which inhibits the septal transpeptidase PBP3 [53,54] but still allows for pre-septal PG synthesis at future cell division sites by class A PBPs, which are recruited by the FtsZ membrane anchors FtsA and ZipA [11]. As expected, aztreonam induced cell filamentation in all strains tested, indicating an inhibition of cell division (Fig 5C). When expressed after aztreonam addition, SddA-sfGFP did not localize at future division sites, indicating that ongoing septum PG synthesis by PBP3 is required for SddA recruitment to midcell (Fig 5C). These results suggest that SddA interacts with one or more divisome proteins, or with septal PG, in a manner dependent on septal PG synthesis.

SddA overexpression phenocopies the removal of septal amidase activators

The above results suggest that SddA localizes at midcell, where it can modulate the activity of EnvC-AmiA/B and/or NlpD-AmiC pairs. If this hypothesis is correct, SddA overexpression should mimic the effects of *envC* or *nlpD* deletion. We tested this hypothesis using *E. coli* mutants defective in the Tol-Pal system, which lyse upon the addition of sub-MIC concentrations of the PBP3-inhibitor aztreonam [55]. We confirmed this phenotype in both, a Δ*tolR* mutant and in cells harbouring TolR D23R, which is unable to harness the proton motive force for the correct functioning of Tol-Pal [56] (Fig 6). The Tol-Pal system coordinates PG synthesis and cell envelope constriction during cell division, suggesting that this phenotype could result from dysregulation of synthetic and hydrolytic PG activities. Additional inactivation of the amidase activators *envC* (or *nlpD*) prevented (or reduced) cell lysis (Fig 6), supporting the idea that amidase activity is misregulated in Tol-Pal-defective cells when PBP3 is inhibited by aztreonam. Similarly, the overproduction of SddA (either native or fused to sfGFP) prevented lysis of Δ*tolR* cells in the presence of the PBP3 inhibitor (Fig 6). This further supports the hypothesis that SddA inhibits amidases or their regulators at midcell.

Mid-cell localisation of plasmid-encoded active SddA causes cell chaining

Since *sddA* is genetically linked to *envC*, and excess production of SddA over EnvC causes cell chaining, we explored potential SddA-EnvC or SddA-FtsX interactions using AlphaFold (S16 Fig). AlphaFold predicted an SddA-FtsX complex

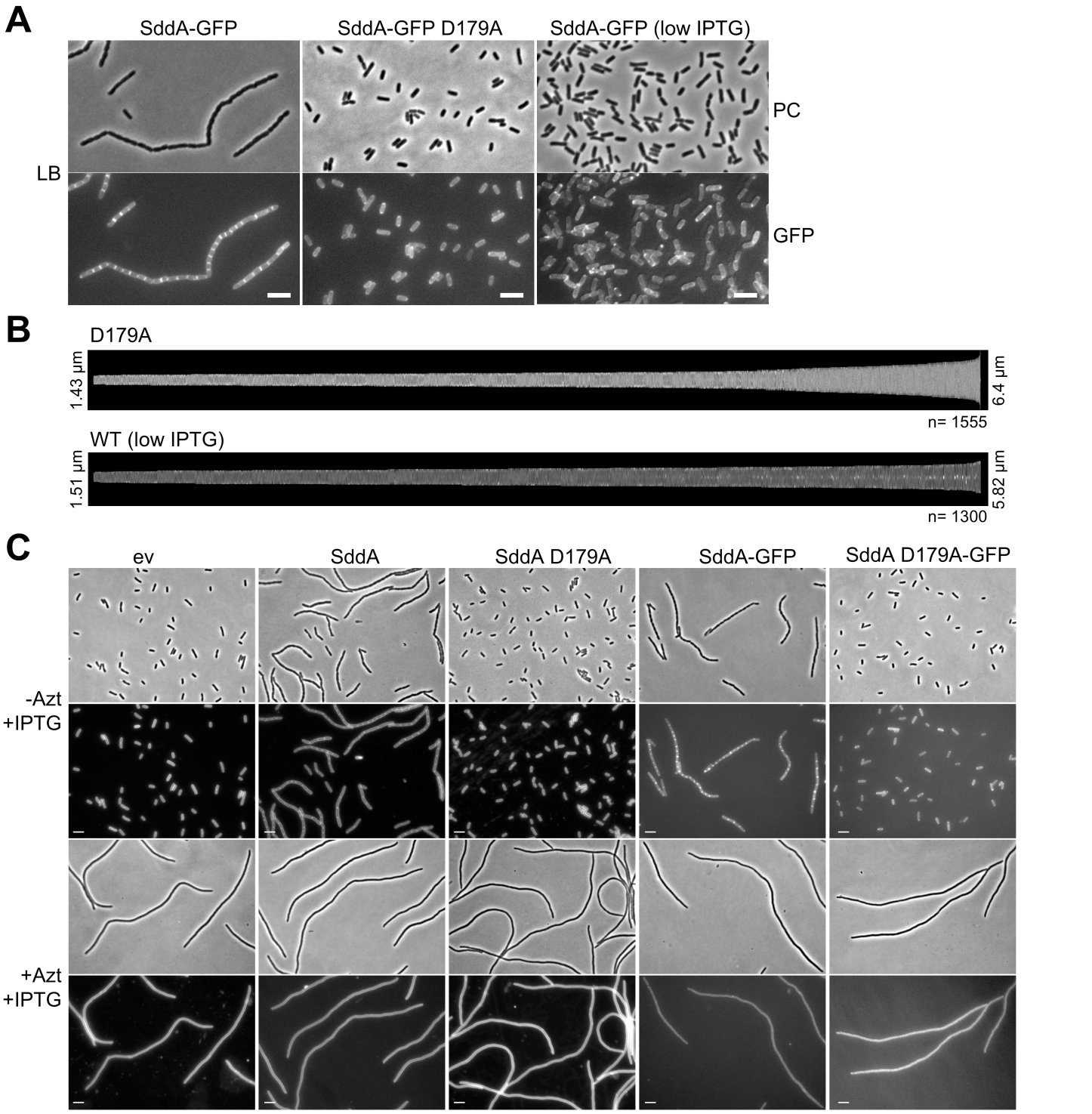

Fig 5. SddA localization at the cell division site depends on septal peptidoglycan synthesis. (A) Phase contrast (PC) and fluorescence microscopy (GFP) images of BW25113 harbouring pMP108 (pGS100 *sddA::sfgfp*; SddA-GFP) and pMP116 (pGS100 *sddA D179A::sfgfp*; SddA D179A-GFP). Cultures were grown in LB with 20 µg ml^{-1} chloramphenicol at 37°C and expression of the fluorescent constructs was induced with 25 µM (indicated as [low IPTG]) or 0.5 mM IPTG for 140 min. Scale bar is 5 µm. (B) Demographs of SddA D179A-GFP (D179A) or SddA-GFP (WT (low IPTG)) localization in cells sorted according to their cell length (from 1.43 µm to 6.4 µm, n = 1555, 0.5 mM IPTG induction for SddA D179A; from 1.51 µm to 5.82 µm, n = 1300, 25 µM IPTG induction for SddA WT). The fluorescence signal of D179A does not show an increase of the intensity at midcell, while the fluorescence

signal of WT at low IPTG does. (C) BW25113 cells harbouring pGS100 (ev), pGS100 encoding *sddA, sddA D179A, sddA::sfgfp,* or *sddA D179A::sfgfp* were grown in LB with 20 μg ml^{-1} of chloramphenicol at 37°C. When OD578 reached 0.1, 1 μg ml^{-1} of aztreonam was added. Expression of the plasmid-encoded constructs was induced 30 min later by addition of 0.5 mM IPTG for 80 min. Samples were imaged by phase contrast and fluorescence microscopy (FM5-95 or GFP). Representative images are shown. Scale bar is 5 μm.

https://doi.org/10.1371/journal.pgen.1011626.g005

(score: 0.338), where SddA binds to the periplasmic porter domain of FtsX, and an SddA-EnvC complex (score: 0.530), where SddA interacts with the coiled-coil region of EnvC. Although the FtsX-SddA model had a relatively low confidence score, both FtsX-SddA and EnvC-SddA models predicted that the SddA residues involved in the interactions are located on the same side as the predicted SddA catalytic active site. Moreover, both models predict D179 of SddA to be involved in contacts with FtsX or EnvC. To test this, we overproduced an alanine-179 variant of SddA and analysed its effects on the phenotypes. Overexpression of SddA D179A failed to rescue the lysis of Δ*tolR* in the presence of aztreonam (Fig 6), suggesting that the mutated protein cannot inhibit amidases. In addition, overexpression of SddA D179A or a SddA(D179A)-sfGFP fusion did not induce cell chaining (Fig 5A). Strikingly, SddA(D179A)-sfGFP failed to localize at mid-cell (Fig 5AB). Finally, we introduced the D179A mutation into His-$SddA^{24\text{-}238}$ and tested the activity of the purified protein *in vitro*. This variant of SddA remained active against denuded strands (S17 Fig), indicating that the D179A mutation does not affect enzymatic activity, and that the lack of effects upon overproduction is not due to a loss of deacetylase activity.

To understand how the D179A change might disrupt the interaction of SddA with EnvC, we performed molecular dynamics simulations of both WT and D179A, which highlighted the differences in residue fluctuations between them (S18 Fig). SddA residues predicted by AlphaFold to form EnvC contacts include 32, 35–36, 55, 59–60, 85–88, 90, 123–124, 154, 177, 179–180, 182, 209 and 211. The D179A change affected the flexibility of some of those residues, with strong rigidification of residues 35, 36, 58, 59 and 177, potentially hindering adaptive binding, and flexibilization of residues 87 and 124, which may further disrupt the interaction by destabilizing the binding interface. Beyond local effects, D179A induced fluctuation changes in residues 174 and 202, suggesting an allosteric disruption of the interaction; while altered dynamics in regions outside the EnvC interface indicate broader effects on protein flexibility. Catalytic regions were unaffected, with minimal fluctuation differences in residues critical for enzymatic activity, in agreement with the fact that SddA D179A is catalytically active (S17 Fig). Overall, the D179A change may disrupt the SddA-EnvC interaction by altering the dynamics of critical contact residues and their surroundings. The combined changes in rigidity and flexibility appear to compromise conformational adaptability and emphasise the role of residue-specific dynamics in mediating these particular protein-protein interactions.

In summary, these results suggest that SddA localization to midcell is important for its effect inhibiting amidases and that this localization requires the interaction with septum components.

SddA also inhibits the activation of AmiC by NlpD

As our results suggest that SddA can inhibit amidase activation at the septum, we tested the effect of SddA on the activity of amidases and their activators *in vitro*. To do this, we performed activity assays with amidase/activator pairs, EnvC-AmiA, ActS-AmiC and NlpD-AmiC, in the presence or absence of His-$SddA^{24\text{-}238}$ (Figs 7 and S19). In the case of EnvC, two versions of this activator were tested: EnvC(LytM), which only contains the AmiA-activating LytM domain, and EnvC(fl), which contains the full mature sequence. Previous work showed that only EnvC(LytM) but not EnvC(fl) activates AmiA and AmiB *in vitro* [21,57]. In control assays, His-$SddA^{24\text{-}238}$ showed no effect on AmiA or AmiC amidases in the absence of their activators (S19C Fig). Surprisingly, His-$SddA^{24\text{-}238}$ showed no effect on ActS-AmiC activity or EnvC(fl)-AmiA activity, but there was a small activation of EnvC(LytM)-AmiA (S19AB Fig). This could indicate that FtsEX is required for the inhibition of EnvC by SddA. In contrast, His-$SddA^{24\text{-}238}$ significantly inhibited NlpD-AmiC activity against PG (Fig 7). Interestingly, neither catalytically inactive His-$SddA^{24\text{-}238}$ H123A nor catalytically active His-$SddA^{24\text{-}238}$ D179A

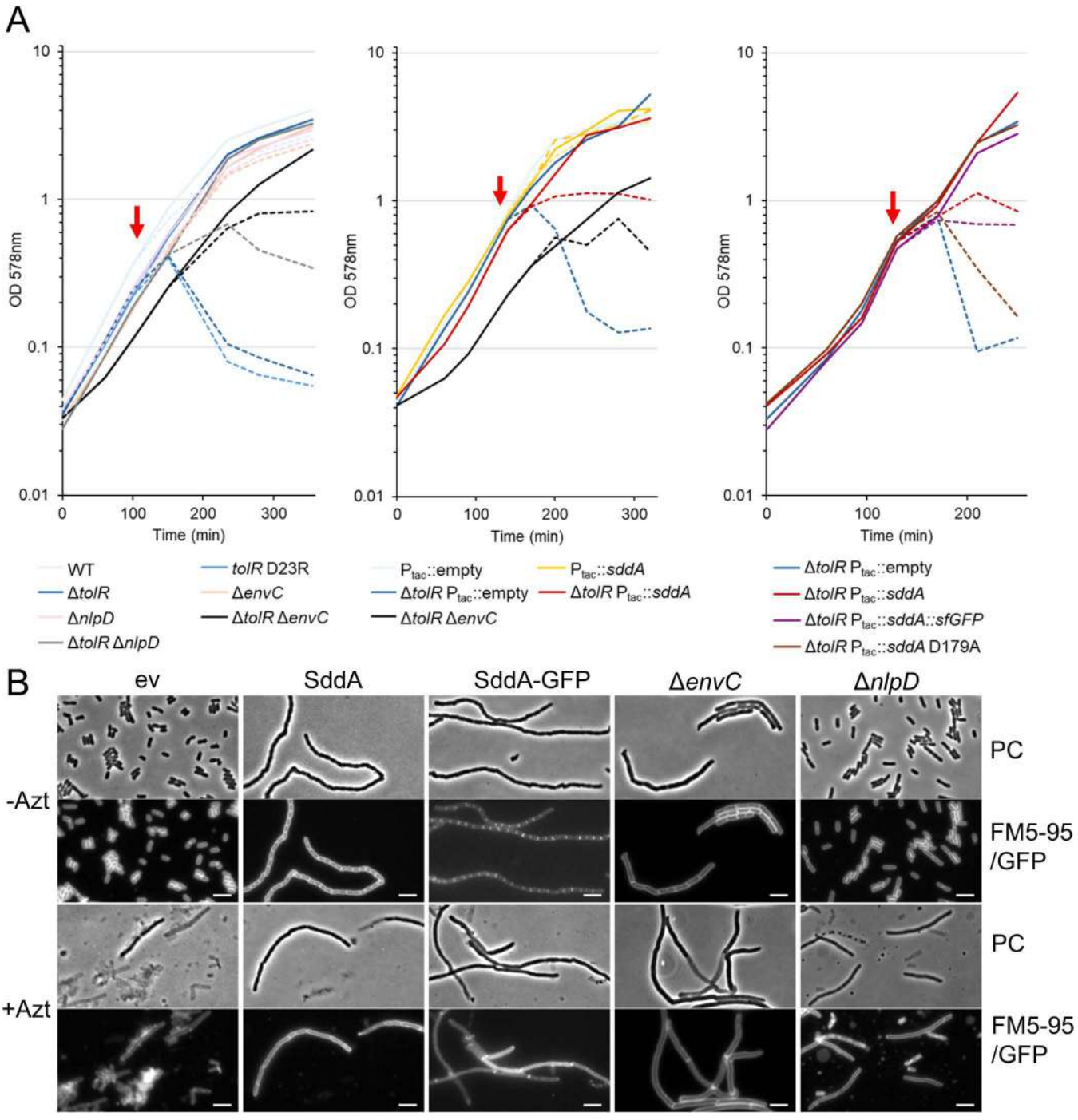

Fig 6. SddA phenocopies the absence of *envC* during the lysis of *tol* defective cells upon septal PG synthesis inhibition. (A) BW25113 (WT), BW25113 Δ*tolR*, and BW25113 *tolR* D23R were grown in LB; BW25113 Δ*nlpD*, BW25113 Δ*envC*, and respective double knockouts with Δ*tolR*, in LB with 50 μg mL^{-1} kanamycin; BW25113 and BW25113 Δ*tolR* harbouring pGS100 and pGS100 *sddA* (and variants), in LB with 20 μg mL^{-1} chloramphenicol. All strains were grown at 37°C. When indicated by a red arrow, cultures were split in two halves and 1 μg ml^{-1} aztreonam was added to one of them (dashed line). In the middle and right panels, overexpression of the plasmid-encoded genes was induced by adding 0.5 mM IPTG when OD578 reached 0.1. (B) Representative phase contrast (PC) and fluorescence microscopy (FM5-95, or GFP in case of SddA-GFP) micrographs of samples taken 110 min after splitting cultures (red arrow) of BW25113 Δ*tolR*::FRT containing the empty vector (ev), pGS::*sddA* (SddA) or pMP108 (SddA-GFP), MPW55 (Δ*envC*) and MPW54 (Δ*nlpD*) cells in absence (-Azt) or presence of aztreonam (+Azt). Scale bar is 5 μm.

https://doi.org/10.1371/journal.pgen.1011626.g006

variants inhibited NlpD-AmiC in this assay (Fig 7), consistent with the lack of cell chaining when these variants are over-produced in cells.

Discussion

PgdA-type PG deacetylases have been found in many Gram-positive bacteria where they have roles in protecting the cell from exogenous PG hydrolases such as lysozyme [27,29,58], autolysin regulation [59], osmotic stability [60], sporulation [61] and virulence [28–30,62]. Gram-negative bacteria have an OM that protects the PG from exogenous hydrolases, and there was no clear evidence for the presence of PgdA-like PG deacetylases. We now identified the first PG deacetylase in

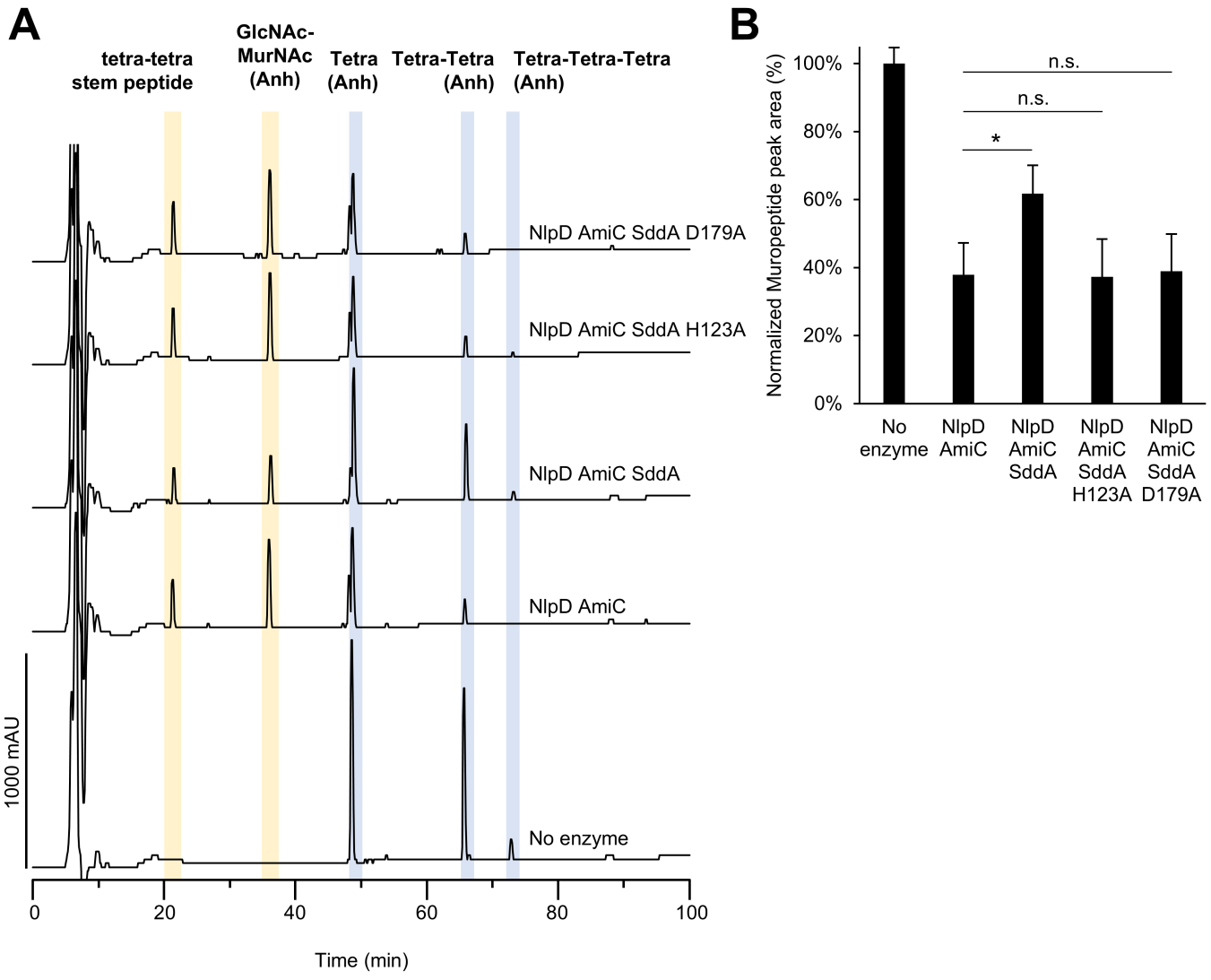

Fig 7. NlpD-AmiC is inhibited by SddA. (A) HPLC-based end point activity assay for NlpD-AmiC in the presence or absence of SddA. Sacculi were incubated with 1 μM AmiC, 1 μM NlpD and in the presence or absence of 2 μM His-SddA$^{24\text{-}238}$ (SddA), His-SddA$^{24\text{-}238}$ H123A or His-SddA$^{24\text{-}238}$ D179A for 30 min at 37°C. Representative chromatograms are shown. Identity of the labelled peaks is shown above and structures are depicted on S19E Fig. (B) Quantification of peak areas for undigested muropeptides (peaks shaded in blue) in (A). Areas are normalized to the ones in the control with no enzyme (100%). Values are average ± SD of three repeats, * p-value < 0.05 and n.s. not significant.

https://doi.org/10.1371/journal.pgen.1011626.g007

a Gram-negative bacterium, *E. coli* that, unlike PgdA, acts specifically on denuded glycan strands and has a role in modulating septum cleaving amidases.

SddA is the first characterized protein from the divergent polysaccharide deacetylase family (PFAM PF04748), although two X-ray crystal structures are available on the PDB database: entries 2NLY corresponding to BH1492 from *Bacillus halodurans* and 2QV5 corresponding to ATU2773 from *Agrobacterium tumefaciens*. Both structures show remarkable similarity to the polysaccharide domain of PgdA. However, only the BH1492 structure contains a Zn^{2+} ion coordinated by four residues (two histidine and two aspartic acid residues) instead of the three in PgdA (two histidine and one aspartic acid residues). These four residues are also present in *E. coli* SddA and here we show that replacing either of the histidine residues or the two aspartic acid residues with alanine(s) abolishes the catalytic activity. Intriguingly, Zn^{2+}-coordinating residues are not present in ATU2773, but this gene still resides in the same operon as an *envC* homologue in *A. tumefaciens*. This might indicate that a catalytically inactive ATU2773 has retained a regulatory function linked to EnvC in this organism (see below).

Link to amidase-mediated septal PG cleavage

The cleavage of the new division septa by peptidoglycan amidases enables Gram-negative bacteria to separate the two daughter cells. The activation of these enzymes occurs from inside the cell via FtsEX-EnvC or the OM via NlpD (or ActS). Here we describe a new potential player in amidase regulation, the enzyme SddA, which we demonstrate to be a denuded glycan strand deacetylase that removes the *N*-acetyl group from Glc*N*Ac residues. In the cell, SddA localizes at the septum where denuded strands are produced during cell division by the amidases. Importantly, our data suggest that SddA induces cell chaining if its expression level exceeds a threshold, a phenotype characteristic of deficient peptidoglycan amidase activity. The presence of *envC* in the same operon as *sddA* in the expression plasmid, reduced the amount of SddA produced upon induction. This suggests that the *envC-sddA* operon structure enables Gram-negative bacteria to adjust the level of SddA to avoid inhibition of amidase activity. Regulation of SddA expression could involve translational coupling by "termination-reinitiation", where the same ribosome translating the upstream gene initiates the translation of a downstream gene with an overlapping or nearby start codon (*envC* stop codon and *sddA* start codon are separated by 3 bp in *E. coli*) [63].

Importantly, SddA overexpression mimicked the phenotype observed upon removal of amidase activators in Tol-Pal deficient cells, further supporting the notion that SddA inhibits amidases *in vivo*. This hypothesis is also supported by the inhibition of purified NlpD-AmiC by SddA. By contrast, we did not observe an inhibition of EnvC(LytM)-AmiA or EnvC(fl)-AmiA by SddA. The inhibitory effect of SddA on EnvC observed in cells, might require FtsEX, which induces the conformation in EnvC capable of activating the amidases in cells. We report that SddA activity is needed for inhibition of amidases, for example the inactive version SddA H123A was unable to produce cell chaining (S12 Fig) or inhibit NlpD/AmiC *in vitro* (Fig 7). We also identified an SddA variant, D179A, that is catalytically active and yet its overexpression does not induce chaining or mimic the effects of removing the amidase activator *envC* in Tol-Pal-deficient cells. SddA(D179A) failed to localize at the septum and did not inhibit NlpD/AmiC *in vitro*. This suggests that inhibition of amidases by SddA does not *only* depend on enzymatic activity but also on the correct mid-cell localisation, where it may interact with amidases or their regulators. The D179A mutation was designed based on structural models of potential SddA/EnvC and SddA/FtsX complexes, suggesting that D179A may disrupt the hypothetical interactions with these or other septal binding partners, such as NlpD or the amidases. However, additional experiments are required to test this hypothesis, including the identification of specific SddA interaction partners at the septum, elucidation of the mechanism by which it interferes with amidase activity or activation, and clarification of the precise role of its enzymatic activity in this process.

Why does the cell deacetylate denuded glycan chains?

Our data are consistent with a model in which SddA modulates a transition of amidase activation from inside the cell in early septation to amidase activation from the OM in late septation (Fig 8). We hypothesize that SddA inhibits NlpD-AmiC

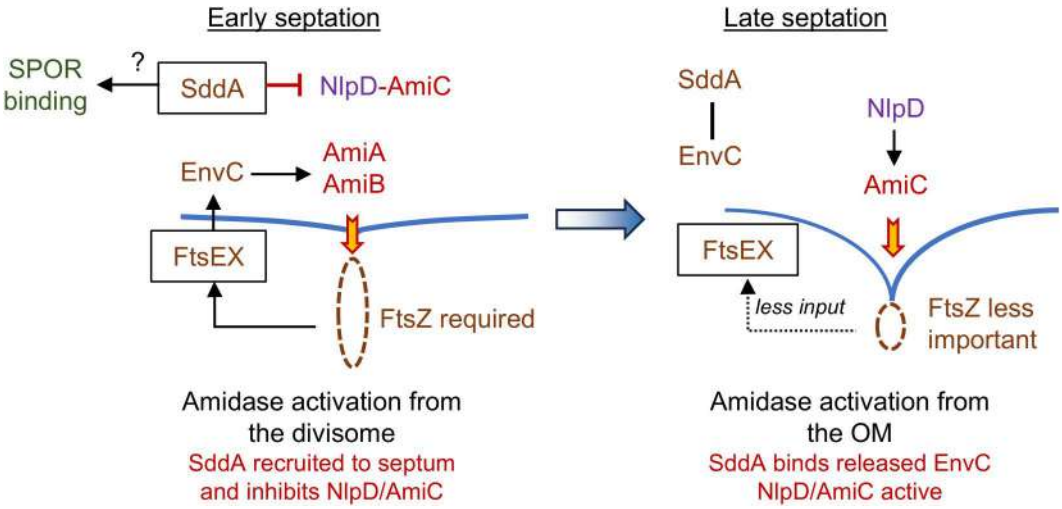

Fig 8. Hypothetical model for the role of SddA in modulating amidase activation in septation. SddA is recruited to the divisome where it inhibits NlpD-AmiC during early septation ensuring that PG hydrolysis is controlled by the divisome from the cytoplasmic membrane. In late septation, FtsEX receives less input from FtsZ, releasing EnvC that competes with NlpD-AmiC for SddA binding. NlpD-AmiC become more active as EnvC-AmiA/AmiB are less active, shifting the control of amidase activation from the CM to the OM. Excessive SddA (but not EnvC-SddA) inhibits amidase activation from the CM and OM, explaining the observed chaining phenotype. The deacetylation of denuded glycan strands likely modulates the binding of SPOR domain proteins and the activities of glycan strand degrading enzymes.

https://doi.org/10.1371/journal.pgen.1011626.g008

during early septation to ensure that PG hydrolysis is controlled mainly by the divisome via FtsEX-EnvC and ultimately FtsZ. In late septation, FtsZ becomes less important and even dispensable, as it departs from the division site before septation is completed, leaving PG synthesis to drive the final stages of septation [64,65]. Consequently, FtsEX-EnvC might become less efficient at amidase activation during this phase. At this point, SddA might leave the septal region, allowing NlpD-AmiC to be activated and shifting control of amidase activation to the OM. Alternatively, more EnvC could be available to interact with SddA, which relieves the SddA-mediated inhibition of NlpD-AmiC thus shifting septum cleavage control to the OM (Fig 8). Because the Δ*sddA* strain does not exhibit a major phenotype, this regulatory mechanism may not be required for *E. coli* growing under laboratory conditions. However, we cannot exclude that SddA plays a more critical role in other species or under growth conditions not examined in this study. Given the widely conserved genetic link between *envC* and *sddA* (Fig 1), SddA-mediated modulation of septum cleavage could provide an advantage for Gram-negative bacteria. SddA might enhance the energy efficiency of cell division by more precisely restricting PG hydrolysis both spatially and temporally. In support of this, the third gene in the *envC-sddA* operon, *gpmM*, encodes for an alternative glycolytic enzyme, establishing a link between PG hydrolysis regulation and central energy metabolism. Further experiments are needed to test these proposed regulatory connections.

SddA function beyond amidases?

SPOR domains bind Glc*N*Ac residues in denuded glycan strands and it remains to be tested whether (partial) deacetylation of the denuded strands affects the binding and/or function of individual SPOR domain proteins. Cells lacking SddA do not exhibit major growth or cell division phenotypes that would be consistent with a loss of function of the essential cell division protein FtsN. Therefore, we hypothesize that FtsN functions largely normally in the absence of SddA-mediated glycan chain deacetylation. Supporting this idea, we observed no difference in the recruitment of the FtsN's SPOR domain (iSPOR) to midcell in the absence of SddA (Fig 2E). However, whether FtsN or other SPOR proteins are affected by

the lack of glycan chain deacetylation under specific conditions, and whether deacetylation alters their affinity for glycan chains or impacts their cellular dynamics, remains to be determined.

Although the underlying mechanism is not fully understood, mutants lacking PG hydrolases form chaining cells and show increased OM permeability. Interestingly, deletion of *sddA* in strains containing only the NlpD or EnvC amidase activators reduced the sensitivity to deoxycholate, indicating a restoration of the OM permeability barrier function. This result is consistent with a role for SddA as an inhibitor of amidase activity and/or activation. In genetic backgrounds with defective amidase activation, removing an inhibitor could enhance amidase function, and hence alleviate OM integrity defects. More puzzling, however, is the deleterious effect of the *sddA* deletion in the Δ*envC* Δ*nlpD* background. This suggests that SddA affects additional factors beyond the known amidases, potentially including other enzymes involved in daughter cell separation, such as the lytic transglycosylase MltB or the muramidase DigH, which have been implicated in septal splitting in the absence of amidases [55].

In conclusion, here we have identified a novel PG-modifying enzyme with an activity, to our knowledge, not previously reported, the deacetylation of denuded PG glycan strands. SddA modulates PG amidases and is widely conserved in Gram-negative bacteria. Future work will investigate the potential links of SddA with SPOR domain proteins and other periplasmic factors involved in cell division and envelope integrity.

Materials and methods

Bacterial strains and growth conditions

Strains used in this study are listed in S1 Table. Bacteria were grown on LB plates or in liquid LB medium (10 g L^{-1} tryptone, 5 g L^{-1} yeast extract, 10 g L^{-1} NaCl for liquid media or 15 g L^{-1} for agar plates), or in LB-Lennox medium, liquid o agar plates (10 g L^{-1} tryptone, 5 g L^{-1} yeast extract, 5 g L^{-1} NaCl) at 37°C or 30°C when indicated. Growth of bacteria for protein expression was in LB, containing antibiotic for selection. Antibiotics were used at the following concentrations: Chloramphenicol (Cam, 20 or 25 μg mL^{-1}); Kanamycin (Kan, 30 or 50 μg mL^{-1}), and Ampicillin (Amp, 100 μg mL^{-1}). Optical density at 578 nm (OD578) was measured with the spectrophotometer UV5 Bio (Mettler Toledo). Optical density at 600 nm (OD600) was measured with the Libra S22 spectrophotometer (Biochrom Ltd).

For cell length measuring of BW25113, Δ*sddA*, Δ*dedD* and Δ*sddA* Δ*dedD* strains (Fig 2C), strains were grown overnight in LB-Lennox at 30°C, diluted 1:100 in fresh medium and grown to an OD578 of 0.4. Cultures were diluted in fresh medium to OD578 of 0.1, and microscopy samples were taken when cultures reached OD578 of 0.3.

For SddA overexpression, BW25113 or deletion mutant derivative cells, containing either pGS100 and its derivatives, were grown overnight at 37°C, diluted 1:100 in fresh medium containing 0.5 mM IPTG and grown to stationary phase. Microscopy samples were taken at mid exponential phase (OD600 of around 0.8).

For the overexpression of SddA with EnvC or NlpD, BW23113 cells harboring either pGS100 or its derivative expressing SddA, along with pBAD24 or its derivative expressing EnvC or NlpD, were grown overnight at 37°C. These cultures were then diluted 1:100 in fresh medium containing 0.5 mM IPTG and 0.2% arabinose and grown to stationary phase. Samples for microscopy were collected during mid-exponential phase when the OD600 reached approximately 0.8.

BW25113 cells containing pGS100 and derivatives were grown overnight at 37°C, diluted 1:100 in fresh medium and grown to OD578 of 0.1. Cell cultures were divided in two halves, adding to one of them aztreonam (1 μg mL^{-1}). After 30 min of incubation at 37°C, overexpression of plasmid-encoded genes was induced adding 0.5 mM IPTG unless indicated otherwise. Microscopy samples were taken 80 min after IPTG induction. For Western blot, samples were taken 140 min after IPTG induction.

For SddA overproduction in Δ*envC* or Δ*ftsX* cells, MPW56 derivatives were grown at 37°C in LB and MP055 ones were grown at 30°C in LB supplemented with 0.2 M sucrose. Overnight cultures were diluted (1:100, MPW56; 1:50, MP055) in fresh medium and grown to OD578 of 0.1. Overexpression of plasmid-encoded genes was induced adding 0.5 mM IPTG. Microscopy samples were taken after 140 min (MPW56) or 230 min (MP055) of incubation with IPTG.

For *tol* defective strains, overnight cell cultures grown at 37°C were diluted 1:100 (1:50, MPW55) in fresh medium and grown to OD578 of 0.1. Overexpression of plasmid encoded *sddA* (and variants) was induced by addition of 0.5 mM IPTG. After 30 min, cell cultures were divided in two halves, adding aztreonam (1 μg mL^{-1}) to one of them. Microscopy samples were taken 140 min after IPTG induction

Construction of strains and plasmids

Strains. MP001 (BW25113 Δ*dedD*::FRT) was obtained by removing the Kan cassette from the corresponding Keio collection single knockout mutant strain by pCP20-encoded Flp recombinase [66,67]. MP005 (BW25113 Δ*sddA*) was obtained by conjugation [68] of recipient BW25113 carrying pACBSR with the donor MFDpir carrying pMP019. Absence of *sddA* was confirmed by PCR using the primers FwupYibQseq and Rv downYibQseq. MP006 (BW25113 Δ*dedD* Δ*sddA*) was obtained by conjugation of recipient MP001 carrying pACBSR with the donor MFDpir carrying pMP019. Absence of *sddA* was confirmed by PCR using the primers FwupYibQseq and Rv downYibQseq. MP055 (BW25113 Δ*ftsX*) was obtained by conjugation of recipient BW25113 carrying pACBSR with the donor MFDpir carrying pMP112, growing them at 30°C on LB 0.2 M sucrose. Absence of *ftsX* was confirmed by PCR using two sets of primers: FwupftsX and RvdownftsX; and FwintftsX and RvintftsX. Growth defects characteristic of *ftsX* inactivation [69] were confirmed in medium with no NaCl (LB 0% NaCl) and were rescued when supplemented with sucrose (LB 0% NaCl 0.2M sucrose) or with NaCl (LB 1% NaCl). MPW54 (BW25113 Δ*tolR*::FRT Δ*nlpD::aph*) was generated by transduction of BW25113 Δ*tolR*::FRT with P1 lysate from the strain BW25113 Δ*nlpD::aph*, and absence of *nlpD* was confirmed by PCR using primers FwupnlpD and RvintnlpD. MPW55 (BW25113 Δ*tolR*::FRT Δ*envC::aph*) and MPW56 (BW25113 Δ*envC::aph*) were constructed by transduction with P1 lysate from BW25113 Δ*envC::aph* of BW25113 Δ*tolR*::FRT and BW25113 strains, respectively, and the absence of *envC* was confirmed by colony PCR using two sets of primers: FwupenvC and RvintenvC, and FwintenvC and RvdownenvC.

Other deletion strains were obtained by moving *kan*-marked alleles from the Keio *E. coli* single gene knockout library [66] by P1 phage transduction [70] or by recombineering using the pKD46 and Kan cassette amplified from pKD4 as indicated [66,67]. Afterwards, the Kan cassette was removed by pCP20-encoded Flp recombinase to generate unmarked deletions with an FRT-site scar sequence [67]. The removal of the *kan* gene was verified by colony PCR. Strains with multiple deletions were generated by sequential P1 transduction or recombineering and *kan* cassette removal.

Plasmids. All template plasmids are listed on S2 Table and oligonucleotide sequences are listed on S3 Table. All mutagenesis (base changes or insertions) steps were performed using the Q5 Site-Directed Mutagenesis Kit (New England Biolabs) according to manufacturer's instructions.

pET28a-HSddA plasmid, encoding for full length mature SddA (residues 24–319) with an N-terminal His-tag, was amplified by PCR from genomic DNA of *E. coli* BW25113 using oligonucleotides YibQ_FW_NdeI and YibQ_REV_NdeI, and cloned into pET28a(+) with the appropriate restriction enzymes. pET28a-HYibQ$^{24\text{-}238}$ was obtained by mutagenesis using primers YibQ_N239stop_FW and YibQ_N239stop_REV, incorporating a stop codon at position 239 in pET28a-HYibQ. pET28a-HSddA$^{24\text{-}238}$ D31A/D32A, pET28a-HSddA$^{24\text{-}238}$ H78A, pET28a-HSddA$^{24\text{-}238}$ H123A and pET28a-HSddA$^{24\text{-}238}$ D179A were obtained by site directed mutagenesis with primers listed in S2 Table.

pGS100-*sddA* was constructed by cloning into the EcoRI-HindIII-digested pGS100 vector a PCR fragment encoding for full length SddA (residues 1–319) amplified from genomic BW25113 DNA using oligonucleotides AP907/yibQ_EcoRI_fw and AP908/yibQ_HindIII_rv.

pGS100-*envC* and pGS100-*envC-sddA* were constructed by cloning into the EcoRI HindIII-digested pGS100 vector a PCR fragment encoding for full length EnvC (residues 1–419) or EnvC-SddA (residues 1–419 and 1–319, respectively) amplified from genomic BW25113 DNA using oligonucleotides AP937/*envC*_EcoRI_fw and AP938/envC_HindIII_rv or AP937/*envC*_EcoRI_fw and AP908/yibQ_HindIII_rv.

pGS100-*FLAG-sddA*, and pGS100-*envC-FLAG-sddA* were obtained by mutagenesis of pGS100-*sddA* and pGS100-*sddA-envC* to insert a FLAG tag at the N-terminus of SddA (after the signal peptide), using primers yibQ_NtFLAG_FW and yibQ_NtFLAG_REV. pGS100-FLAG-*sddA* H123A was obtained by mutagenesis of pGS100-FLAG-*sddA* with primers sddA_H123A_F and sddA_H123A_R.

pBAD24-*nlpD* was constructed by cloning into the EcoRI-HindIII-digested pBAD24 vector the PCR fragment encoding for full length NlpD (residues 1–379) amplified from genomic BW25113 DNA using oligonucleotides AP970/NlpD_EcoRI_fw and AP998/NlpD_HindIII_rev. The inserts were verified by sequencing.

pBAD24-*envC* was constructed by cloning into the EcoRI HindIII-digested pGS100 vector a PCR fragment encoding for full length EnvC (residues 1–419) amplified from genomic BW25113 DNA using oligonucleotides AP937/*envC*_EcoRI_fw and AP938/envC_HindIII_rv.

pET28a-His-AmiD was generated by two PCR fragments: an amplified product obtained from pET28a and the primers FwLICHisAmiD(V) and FwLICHisAmiD(V), and an amplified product obtained from BW25113 genomic DNA and the primers FwLICHisAmiD(I) and FwLICHisAmiD(I). Same volumes of each PCR fragments were mixed, heated to 98°C and cooled down to room temperature. The DNA mixed was digested with DpnI and transformed into DH5α competent cells. pMP018 was generated by a similar procedure, using pGEC and the primers FwpGECLIC and RvpGECLIC, and an amplified product obtained from BW25113 genomic DNA and the primers FwupYibQLIC and RvdownYibQLIC. pMP107 was generated by a similar procedure, using pGEC and the primers FwpGECLIC and RvpGECLIC, and an amplified product obtained from BW25113 genomic DNA and the primers FwupFtsXLIC and RvdownFtsXLIC. pMP108 was obtained by the same procedure, using pGS100-sddA and the primers FwpGS100LIC and RvyibQLIC, and pAND101 and the primers FwyibQsfGFPLIC and RvsfGFPLIC. pMP019 was obtained by site-directed mutagenesis (SDM) over pMP018, using the primers FwYibQSDM and RvYibQSDM, and an annealing temperature of 60°C. pMP110 was obtained by site-directed mutagenesis (SDM) over pGS100-*sddA*, using the primers FwSDMyibQD179A and RvSDMyibQD179A, and an annealing temperature of 61°C. pMP112 was obtained by the same SDM procedure, using pMP107 as template and the primers FwdelftsXSDM and RvdelftsXSDM, and an annealing temperature of 62°C. pMP116 was obtained by the same SDM procedure, using pMP108 as template and the same primers used for pMP110.

Purification of proteins

His-SddA variants. Versions of SddA (His-SddA, His-SddA$^{24\text{-}238}$ or the D31A/D32A, H78A, H123A and D179A mutants) were expressed in *E. coli* BL21(DE3) from freshly transformed cells using the corresponding plasmids (S2 Table). 1 L of LB containing kanamycin and auto-induction mix (0.5% glycerol, 0.05% glucose, 0.2% lactose) was inoculated with 10 mL of an overnight starting culture in LB. Cultures were incubated for 24 h at 20°C. Cells were harvested a centrifugation at 7000 × g for 10 min at 4°C. Cell pellets are homogenised in lysis buffer (50 mM Tris-HCL, 1 M NaCl, 10% glycerol, pH 8.0) supplemented with EDTA-free protease inhibitor cocktail tablets (Roche), 2 mM PMSF and DNAse I. Cells were lysed by sonication on ice for 4 min at 70% power, with 15 sec pulses and 40 sec rests between pulses. The lysates were pelleted by centrifugation at 130,000 × *g* for 1 h at 4°C. The supernatant was applied to 2 mL of Ni^{2+}-NTA beads (Novagen) equilibrated in buffer A (25 mM Tris pH 7.5, 500 mM NaCl) supplemented with 10 mM imidazole and incubated for 1h at 4°C. Beads were washed 5 times with cold buffer A supplemented with 50 mM imidazole and the protein was eluted with 3 mL buffer A supplemented with 500 mM imidazole. The eluted protein was analysed by SDS-PAGE and the purest fractions were pooled and extensively dialysed against buffer B (25 mM Tris pH 7.5, 500 mM NaCl, 1 mM EDTA, 10% glycerol). The protein was finally concentrated using filter concentrators with a 10,000 MWCO cut-off, the concentration was measured with a BCA protein concentration kit (Thermo), aliquoted and stored at -80°C. For detection of truncated His-tagged SddA, soluble and insoluble fractions obtained after sonication and centrifugation of cells, where analysed by SDS-PAGE followed by Western blot and immunodetection using anti-His HRP-conjugated antibody (A7058, Sigma).

AmiD. A His-tagged version of AmiD without its signal peptide (residues 18–276) was purified using plasmid pET28a-AmiD (S2 Table). The purification protocol was adapted from reference [71]. Briefly, freshly transformed BL21(DE3) cells were used to prepare an overnight starting culture in LB with Kanamycin at 37°C. 2 L of LB with Kanamycin were inoculated with 1:100 starting culture and incubated at 37°C until OD578 reached 0.4. Protein expression was induced by addition of 1 mM IPTG for 3 h at 37°C. Cells were harvested by centrifugation at 7,000 × *g* for 10 min at 4°C and resuspended in 40 mL buffer A (25 mM Tris-HCl, 150 mM NaCl, pH 8.5) supplemented with EDTA-free protease inhibitor cocktail tablets (Roche), 2 mM PMSF and DNAse I. Cells were disrupted by sonication on ice for 4 min at 70% power, with 15 s pulses and 40 s rests between pulses, and cell debris was removed by centrifugation at 130,000 × *g* for 1 h at 4°C. The supernatant was applied to 2 mL of Ni^{2+}-NTA beads (Novagen) equilibrated in buffer A supplemented with 10 mM imidazole and incubated for 1 h at 4°C. Beads were washed with 10 mL each of buffer A supplemented with 10, 20, 50, and 75 mM imidazole and the protein was eluted with 3 mL each of buffer A supplemented with 100, 150, 200, and 500 mM imidazole. The elution was analysed by SDS-PAGE and the best fractions were pooled and dialysed against buffer A for 2h. Then 1 unit mL^{-1} of thrombin (Novagen) was added, and dialysis against buffer A was continued overnight. Dialysis buffer was switched to buffer C (25 mM Tris-HCl pH 8.5) for 30 min and 30 additional min after a fresh buffer change. The protein was the further purified by anion exchange using a 5 mL HiTrap Q (Cytiva) column equilibrated in buffer C. The protein was eluted with a 50 mL gradient from 0 to 100% buffer D (25 mM Tris-HCl, 1 M NaCl, pH 8.5). The elution was analysed by SDS-PAGE and the best fractions were pooled. After addition of 10% glycerol, samples were aliquoted and stored at -80°C. Protein concentration was measured by UV absorbance using an extinction coefficient at 280 nm of 50,880 $M^{-1\ cm-1}$.

MltA. MltA was purified from *E. coli* 122-1 bearing plasmid pMSS [72], which encodes for a soluble version of MltA without the signal peptide (residues 1–20) and the N-terminal Cys switched for Ala. The purification protocol was adapted from [72]. Briefly, 2 L of LB with Kanamycin were inoculated with 1/100 of a starting culture and incubated at 37°C until OD578 reached 0.3. Protein expression was induced by addition of 1 mM IPTG and cells were incubated for 90 min at 37°C. Cells were harvested by centrifugation at 7,000 × *g* for 10 min at 4°C and resuspended in 40 mL buffer A (25 mM Na-acetate pH 5.2, 10 mM $MgCl_2$) supplemented with EDTA-free protease inhibitor cocktail tablets (Roche), 2 mM PMSF and DNAse I. Cells were disrupted by sonication on ice for 4 min at 70% power, with 15 s pulses and 40 s rests between pulses, and cell debris was removed by centrifugation at 130,000 × *g* for 1 h at 4°C. The supernatant was applied to a 5 mL of HiTrap SP FF column equilibrated buffer A. The protein was eluted with a 45 mL gradient for 0–100% of buffer B (buffer A with 1 M NaCl). Fractions were analysed by SDS-PAGE and the best ones were pooled, concentrated, and further purified by size exclusion chromatography using a Superdex 200 16/600 pg column using buffer C (buffer A with 0.5 M NaCl). Elution was analysed by SDS-PAGE and the best fractions were pooled, concentrated, aliquoted and stored at -80°C. Protein concentration was determined by UV absorbance using an extinction coefficient at 280 nm of 1.348 $(g/L)^{-1}$.

Other proteins. The following *E. coli* proteins were purified following published protocols: AmiA, AmiC, NlpD, and EnvC(LytM) [57]; EnvC(fl) and ActS [21]; PBP1B S510A [73], LpoB(sol) [74].

PG isolation and analysis

PG was isolated from *E. coli* cells and analysed by reversed-phase HPLC as described [39]. For mass-spec analysis of Glc*N*Ac-Mur*N*Ac and Glc*N*-Mur*N*Ac in *E. coli* BW25113 WT and Δ*sddA* PG, PG was digested in MS-compatible buffer (10 mM NH_4HCO_2 at pH 4.8) using MltA previously dialysed in the same digestion buffer. Reactions contained 15 µg of MltA per 10 µL (150 µg) of PG and were incubated for 36 h at 37°C. Samples were then boiled for 10 min, centrifuged for 15 min at 17,000 × *g* and the supernatant concentrated and analysed by LC/MS.

SddA activity assay against radiolabelled denuded glycan strands

Unlabelled lipid II and [^{14}C]Glc*N*Ac-labelled lipid II were prepared as published [75,76]. First, radiolabelled glycan strands were prepared by polymerization of ^{14}C-labelled lipid II with a TPase defective mutant of PBP1B (PBP1B S510A).

Reactions contained 45 μM lipid II and 0.5 μM PBP1B S510A in 50 mM Hepes pH 7.5, 150 mM NaCl, 0.05% Triton X-100, 10 mM $MgCl_2$. After incubation for 90 min at 37°C, samples were boiled for 5 min and digested with NlpD + AmiC to produce denuded glycan strands. These reactions contained 2 μM AmiC, 2 μM ActS, in the same buffer as the PBP1B reactions with the addition of 1 mM $ZnCl_2$, and were incubated for 2 h at 37°C and boiled for 5 min. Radiolabelled denuded strands were either incubated with His-SddA and next digested with cellosyl to break chains into smaller oligosaccharides for HPLC analysis or first digested with cellosyl producing oligosaccharides and then incubated with SddA. In the first case, strands produced from 2.25 nmol of ^{14}C-labelled lipid II (15,000 dpm) were incubated with or without 10 μM His-SddA for 3 h 30 min at 37°C in the same buffer as NlpD + AmiC reactions, boiled for 5 min and then digested with 35 μg ml^{-1} cellosyl in 20 mM sodium phosphate at pH 4.8 overnight at 37°C. In the second case, the same amount of radiolabelled strands were digested with 43 μg ml^{-1} cellosyl in 20 mM sodium phosphate at pH 4.8 and then incubated with or without 10 μM His-SddA overnight at 37C in the same buffer as above. In both cases final samples were boiled for 10 min, centrifuged for 15 min at 17,000 × *g* and the supernatant was reduced with sodium borohydride and analysed by HPLC as previously described [77].

SddA activity assays against PG

For assays of SddA with PG, 10 μL (~150 μg) of isolated PG from *E. coli* MC1061 was incubated with or without 10 μM His-SddA in the presence of 50 mM Hepes pH 7.5, 100 mM NaCl, 0.05% Triton X-100 for 16 h at 37°C and boiled for 10 min. Next, samples we digested with 88 μg ml^{-1} cellosyl in 20 mM sodium phosphate at pH 4.8 overnight at 37°C. For assays of SddA with muropeptides, 20 μl (~150 μg) of isolated PG from *E. coli* MC1061 were first digested with 0.14 mg mL^{-1} cellosyl in 20 mM sodium phosphate at pH 4.8 overnight at 37°C. These samples were then split in two and incubated with or without 10 μM His-SddA in the same conditions as above. In both cases samples were boiled for 10 min, centrifuged for 15 min at 17,000 × *g* and the supernatants were reduced with sodium borohydride and analysed by HPLC as previously described [77].

SddA activity assays against denuded strands

Assays with muramidase-digested denuded strands. First, denuded strands were prepared by digesting PG with AmiC and ActS (4 μM each) in 50 mM Hepes, ~ 150 mM NaCl, 0.05% Triton, 1 mM $ZnCl_2$, for 16 h at 37°C. After boiling reactions for 10 min, denuded strands were digested with cellosyl (30 μg ml^{-1}) in 20 mM sodium phosphate at pH 4.8 for 16 h at 37°C. After boiling reactions for 10 min, the cellosyl-digested denuded strands were incubated with or without 10 μM His-SddA in the same buffer as the amidases for 24 h at 37°C. Final reactions were boiled again for 10 min, centrifuged for 15 min at 17,000 *g* and the supernatant was analysed by HPLC without reduction (see below).

Assays with denuded strands followed by lytic transglycosylase digestion. Denuded strands were prepared by digesting *E. coli* MC1061 or BW25113Δ6LDT PG with AmiD. Digestions were performed with 4 μM AmiD in 20 mM Hepes pH 7.5, 0.5 mM $ZnCl_2$, incubating for 16 h at 37°C. 0.2 nmol of enzyme were added per 10 μL (~150 μg) of purified PG. Samples were boiled for at least 5 min before the next step. SddA reactions included 5 μM of purified SddA and 10 μL of digested PG (50 μL for AmiD reactions) in a total volume of 100 μL. Buffer was 20 mM Hepes pH 7.5, ~ 150 mM NaCl and 0.25 mM $ZnCl_2$. Reactions were incubated at 37°C for 24 h and stopped by boiling for 5 min. For analysis, samples were digested with MltA to produce anhydro-disaccharide units. 4 μM MltA and 20 mM sodium phosphate buffer at pH 4.8 were added to SddA reactions, bringing total volume to 150 μL, and incubated for 16 h at 37°C, boiled for 5 min, centrifuged for 15 min at 17,000 × *g* and the supernatant was analysed by HPLC (see below).

HPLC analysis of SddA reaction products. HPLC analysis was done using a Prontosil 120–3-C18 AQ reversed-phase column (250 × 4.6 mm, 3 μm particle size) and a HPLC apparatus with binary pump system, UV detector and automatic fraction collector. The column temperature was set at 55°C. A 3 h gradient from 0 to 15% acetonitrile in 0.1% formic acid was used for elution. When indicated peaks were isolated by automatic fraction collection and analysed by mass spectroscopy.

Amidase activity assays

Assays contained 10 µL (~150 µg) of isolated PG from *E. coli* MC1061 or *E. coli* BW25113Δ6LDT as indicated. Reactions NlpD-AmiC assays contained 1 µM of each protein, while for EnvC-AmiA and ActS-AmiC reactions contained 2 µM of each protein. SddA was added as twice the concentration of the amidase and activator. Reaction buffer was 20 mM Hepes pH 7.5, 100 mM NaCl, 0.1 mM $ZnCl_2$, 0.05% Triton X-100. Reactions were performed in a 100 µL volume and were incubated at 37°C for 30 min (NlpD-AmiC), 2 h (EnvC-AmiA) or 1 h (NlpD-AmiC). Reactions were stopped by boiling for 5 min. For analysis, samples were digested with MltA to produce anhydro-disaccharide units and analysed by HPLC as described above for SddA assays. At least two repeats were performed per condition. The areas of muropeptide peaks still present in reactions were quantified and analysed relative to the same peaks in control reactions with no amidases.

Western blot and immunodetection of FLAG-tagged SddA

To detect FLAG-SddA from pGS100-derived plasmids, BW25113 cells harbouring the indicated plasmids were grown in LB with 25 µg mL^{-1} chloramphenicol at 37°C to an OD600 of 0.1 and 0.5 mM IPTG was added. 1 mL cell samples were taken after 140 min and 1 ml cell samples were taken, washed twice with PBS and resuspended in 2 × SDS-PAGE loading buffer at an OD600 of 25. Cells were then boiled for 10 min and diluted 1:1 with PBS. 10 µl were loaded on 12% polyacrylamide gels and analysed by SDS-PAGE followed by Western blot and immunodetection. Anti-FLAG antibody (1:1,000) (F3165, Sigma) and HRP-conjugated Goat anti-mouse IgG (1:5,000) (Dako, Germany) were used as primary and secondary antibody, respectively. Western Blots were developed using ECL Prime Western Blotting System (GE Healthcare) and imaged with ImageQuant LAS4000 (GE Healthcare Biosciences).

Western blot and immunodetection of GFP fusion proteins

Indicated cell cultures (10 mL) were centrifuged at 4°C (3,200 × *g*, 10 min) and the pellet was resuspended in 300 µL PBS sterile. Cells were disrupted by sonication (30 s, cycle 0.6, 60% amplitude) using a Sartorius LABSONIC M. Protein extract concentration was determined using Pierce BCA Protein Assay Kit (ThermoScientific). After addition of SDS loading buffer, the protein extracts were boiled at 95°C for 10 min. Fifteen µg of each sample were loaded on 12% polyacrylamide gels and analysed by SDS-PAGE followed by Western blot and immunodetection. Anti-GFP antibody (1:10,000) (A-6455, Invitrogen) and anti-rabbit HRP-IgG (1:5,000) (A8275, Sigma–Aldrich) were used as primary and secondary antibody, respectively. Western Blots were developed using ECL Prime Western Blotting System (GE Healthcare) and processed with Amersham Imager 680.

Microscopy. S7, S9 and S12 Figs.

Cells were grown to the indicated optical densities and in the indicated media and conditions. When indicated, 500 µL samples were taken and fixed by addition of 8% paraformaldehyde and 0.01% glutaraldehyde and incubation for 15 min at room temperature and 30 min on ice. Cells were then washed twice with 1 mL phosphate buffer saline (PBS) at 4°C and stored in PBS at 4°C until use.

Fixed cells were spotted on 1% agarose pads containing 3 µg ml^{-1} FM5–95 membrane dye (ThermoFisher) and deposited on microscope slides and sealed with a glass coverslip (VWR or Fisher Scientific). Slides were visualized using a Nikon Eclipse Ti equipped with a Nikon Plan Apochromat 100x oil objective, a Cool LED pE-4000 light source, a Photometrics BSI camera and NIS-Elements software. For FM5-95 fluorescence, a Chroma 49008 filter-set was used (EX560/40, DM585lprx, EM630/75).

Figs 2C, 5, 6 and S15.

1.5 mL of indicated samples were centrifuged (16,000x*g*, 2 min) and the pellet was resuspended in 1 mL sterile PBS. After another centrifugation, cell pellets were resuspended in 12.5 µL of PBS and 12.5 µL of 3% paraformaldehyde (diluted in PBS) for cell fixation and kept at 4°C until microscopy analysis. When indicated 3 µg mL^{-1} FM5–95 dye was

added to the agarose pads. Cells samples were analysed in the Advanced Light Microscopy Facility at the Centro de Biología Molecular Severo Ochoa (Madrid, Spain). Images were acquired on a Zeiss Axiovert 200M widefield inverted system. A Zeiss EC Plan-Neofluar 100x 1.3 NA Ph3 oil immersion objective was used with Zeiss Inmersol 518F (n = 1.518) oil. Metamorph 7.10.5.476 was used for image acquisition, saving data as .tif formatted files. Fluorescence was sequentially excited with a Spectra-X Lumencor, with filters 470/24 and 575/25 for excitation of sfGFP fusions and FM5–95, respectively. Emission was collected on a sCMOS PCO edge 4.2 bi camera with 16-bit depth, 0.003969 μm^2 pixel size and at 1024x1024 pixel resolution (applying a 2x2 binning). sfGFP and FM5–95 emission signals were collected through a 514/32 and 595–34 emission filters, respectively. For Fig 2C, a Zeiss Plan-Apochromat 63x 1.4 Oil DIC M27 immersion objective was used with Zeiss Inmersol 518F (n = 1.518) oil. Metamorph 7.10.5.476 was used for image acquisition, saving data as .tif formatted files. Fluorescence was sequentially excited with a Spectra-X Lumencor, with filter 575/25 for excitation of FM5–95. Emission was collected on a sCMOS PCO edge 4.2 bi camera with 16-bit depth, 0.003969 μm^2 pixel size and at 2048x2048 pixel resolution (applying a 1x1 binning). FM5-95 emission signals were collected through a 595–34 emission filter.

Images were analysed by segmentation with Omnipose [78] and measurement of cell parameters (length along the cell axis and averaged width along the cell axis) using custom-made scripts. Demographs for SddA(D179A)-sfGFP localization were built by plotting the normalized fluorescence intensity along the cell axis using customs scripts. Each intensity profile along the cells axis was calculated by addition of the fluorescence intensity of 5 pixels perpendicular to each position along the cell axis (I_i). The normalized intensity (I_i^{norm}), and intensity profiles were normalized by:

$$I_i^{norm} = I_i \times \frac{n}{\sum_0^n I_i}$$

where n indicates the length of the profile. For Fig 2C, the violin plots, the average lengths and standard deviations were obtained by analysis of the data with CellDataAnalyser.

Figs 4, S10, S11, S14.

Cells were grown in LB-Lennox containing the opportune antibiotics and 0.5 M IPTG. When indicated, a total amount of cells equal to 3 OD were sampled and fixed in 2.8% formaldehyde and 0.04% glutaraldehyde. Cells were incubated for 30 min at 37°C, with shaking, washed with PBS, resuspended in 0.5 mL of PBS and stored at 4°C until use [79]. Fixed cells were stained with 5 μg ml^{-1} FM5–95 membrane dye (ThermoFisher) and 1 μg mL^{-1} DAPI DNA dye (Sigma), deposited on microscope slides and sealed with a glass coverslip (VWR or Fisher Scientific). Slides were visualized using a Zeiss LSM 900 equipped with C Plan-Apochromat63x/1.4 Oil DIC (WD = 0.14 mm), PALM MicroLaser Systems, AxioCAM ICc1 camera and PALM ROBO-software.

Fig 2D.E.

BW25113 and BW25113 Δ*sddA*::FRT were transformed with pCH-ss^{dsbA}-sfGFP-iSPOR (pAP674) to create strains AP698 and AP699, respectively. This plasmid is a derivative from pJL427 encodes the isolated SPOR domain of FtsN, tagged with sfGFP in its N-terminus, and with the signal peptide sequence from *dsbA* for periplasmic export, under control of an IPTG-inducible promoter [80]. Cells were grown in EZ rich defined medium (EZRDM) [81] containing 150 μg mL^{-1} chloramphenicol (EZRDM+Chlor) at 37°C overnight to saturation. In the morning 1 μL of culture was diluted into 3 mL of EZRDM+Chlor and 100 μM IPTG to induce expression of sfGFP-iSPOR. Cells were grown to an OD600 ~ 0.25-0.40 during which time 500 μL cells were obtained and fixed using paraformaldehyde (2.8%) and glutaraldehyde (0.04%) in EZRDM for 15 min followed by washing three times in PBS by repetitive centrifugation (11,000 × *g* for 5 min). Cells were then imaged on a 3% PBS agarose pad using a 100 × 1.49 NA oil-immersion objective (Olympus). The light was focused onto the chip of an EMCCD camera (iXon Ultra 897, Andor Technology) with a final pixel size of 100 × 100 nm. To obtain the midcell intensity we used a 3 pixel line width to measure the intensity at the midcell (septa) and subtracted the

intensity at the quarter position (background). The median midcell intensity of the WT sample (AP698) for each biological replicate was then used to normalize the midcell intensities values of AP698 and AP699 resulting in "relative midcell intensity".

Analysis of SddA conservation. We used the AnnoTree database [44] to study the conservation of SddA homologues within bacteria and the genetic link between EnvC and DpaA. This database contains a set of archaeal and bacterial genomes which are completely sequenced and consistently annotated with PFAM, KEGG and TIGRFAM annotations [44]. To find SddA homologues, we searched for genes annotated with either PFAM number PF04748 (divergent polysaccharide deacetylase) or KEGG number K09798 (YibQ-like, uncharacterized protein), obtaining 7174 sequences in total. EnvC analogues were identified as genes annotated with KEGG number K22719 (EnvC; murein hydrolase activator) that were not also annotated as any of the KEGG numbers for other LytM activators in *E. coli* (K19304, K06194 or K12943 for MepM, NlpD or YgeR), obtaining 17185 sequences. GpmM homologues were identified as genes annotated with TIGRFAM number TIGR01307 (phosphoglycerate mutase (2,3-diphosphoglycerate-independent)), obtaining 17651 sequences. Finally, AmiC homologues were identified as genes annotated with either KEGG number K01448 (AmiABC; *N*-acetylmuramoyl-L-alanine amidase) or PFAM number PF01520 (N-acetylmuramoyl-L-alanine amidase) that also had a PF11741 (AMIN domain) annotation, obtaining 10499 sequences. The number of proteins of each type per genome was counted using custom Python scripts, and the generated data sets were represented along a phylogenetic tree of all genomes in AnnoTree using iTOL [82]. The localization within the genome of each of the identified sequence was obtained from the downloaded Annotree SQL database and analysed with custom scripts. For each pair of homologues analysed (EnvC + SddA, EnvC + AmiC or SddA + AmiC), genomes containing both homologues were identified and the pair of genes closest together within the same chromosome was selected, counting the number of times the closest pair was on the same strand and the distance in base-pairs between them. The scripts to perform this analysis are available upon request.

Protein structure and protein-protein interaction modeling. Protein structure models and protein-protein interaction models were generated using a local installation of AlphaFold (AlphaFold v2.3.1) [83,84]. Amino acid sequences of the proteins of interest were submitted in FASTA format, following the server's input guidelines. AlphaFold utilizes a deep neural network architecture trained on structural data from the Protein Data Bank (PDB) [85] and multiple sequence alignments to predict protein structures, including protein-protein interactions. For each protein pair, five models were generated, and the highest-confidence model, based on AlphaFold's predicted *ranking_score* which is calculated from the predicted template modeling (pTM) score and the interface predicted template modeling (ipTM) score among other metrics.

The Predicted Aligned Error (PAE) matrix provides a visual representation of the predicted positional accuracy between residues in the modeled protein complex. Each cell in the matrix represents the estimated alignment error (in Å) between pairs of residues across the protein structure, as predicted by AlphaFold. The matrix is color-coded, where darker shades indicate lower predicted alignment errors and higher model confidence, and lighter shades denote areas of greater uncertainty in alignment.

In our analysis, the PAE matrix was used to assess the reliability of inter-protein and intra-protein contacts within the predicted complex. Low error regions, typically appearing along the diagonal of the matrix, correspond to structurally stable segments of each protein. In contrast, off-diagonal regions with low PAE values are indicative of high-confidence inter-protein interactions, suggesting specific interaction sites or binding interfaces. Regions with high PAE values highlight areas of structural flexibility or uncertainty, which may correspond to disordered regions or low-confidence interactions.

Molecular dynamics simulations. Molecular dynamics (MD) simulations were performed for the wild-type SddA protein (WT) and its D179A mutant using five independent replicates for each system. Modeled structures were obtained using AlphaFold. The protonation states of ionizable residues were determined prior to molecular dynamics simulations using the H++ server [86] at pH 7.4. This tool computes residue protonation based on pKa predictions, considering

the influence of the surrounding environment on each residue's ionizable groups. The calculated protonation states were subsequently used to ensure an accurate representation of the protein's charge distribution under the simulation conditions. The system was prepared using the *tleap* module of AmberTools [87]. The protein structure was parameterized using the ff19SB force field [88], and the system was solvated in a triclinic box of OPC water [89] molecules, ensuring a minimum distance of 10 Å between any protein atom and the edge of the box. Sodium and chloride ions were added at random positions to achieve a neutral system and an ionic concentration of 0.15 M. To enable the use of a 4 fs integration timestep during the production phase, the hydrogen mass repartitioning (HMR) [90] technique was applied using the *parmed* module of AmberTools [91]. This method redistributes part of the hydrogen atom masses to their bonded heavy atoms, effectively increasing the hydrogen mass and allowing for a longer integration timestep without compromising simulation stability. The modified topology files were used in all subsequent simulations.

The MD protocol consisted of four phases: energy minimization, heating, equilibration, and production. (i) **Energy Minimization:** This was done in three stages. First, only water molecules were minimized; second, water and ions (excluding hydrogens) were minimized; and third, the full system was minimized. Steepest descent was used for the initial 500–1,000 steps, followed by conjugate gradient minimization. Periodic boundary conditions with an isotropic barostat were applied throughout. (ii) **Heating:** The system's temperature was gradually increased from 100 K to 300 K over 200 ps, using a timestep of 1 fs. A Langevin thermostat [17,92] with a collision frequency of 10 ps^{-1} controlled the temperature. The simulation was at constant volume, with harmonic restraints applied to the backbone and beta-carbon atoms to stabilize the solute. (iii) **Equilibration:** This phase involved 10 steps of 100 ps each using a time step of 1 fs, under constant pressure and temperature. The temperature was kept at 300 K using a Langevin thermostat, and pressure was controlled by a Monte Carlo barostat [93]. A harmonic restraint was applied to alpha-carbon atoms with decreasing force constants. Nonbonded interactions were treated with a 9 Å cutoff, and electrostatics were handled using the particle mesh Ewald (PME) method [94]. (iv) **Production**: The simulation ran for 60 ns with a 4 fs timestep. The temperature was maintained at 300 K using a Langevin thermostat, and pressure was controlled by a Monte Carlo barostat. Electrostatics were treated with PME, and nonbonded interactions had an 11 Å cutoff. Hydrogen mass repartitioning (HMR) enabled the 4 fs timestep. Center-of-mass translation and rotation were removed every 25 ps, and energy, trajectory, and restart files were recorded at 25 ps intervals to ensure accurate sampling during the production phase.

Trajectory analysis was performed using cpptraj [95], from AmberTools suite of programs, focusing on root mean square deviation (RMSD) across the simulation and per-residue root mean square fluctuation (RMSF). Data were visualized using R to evaluate the structural stability and flexibility of both systems.

Supporting information

S1 Fig. Verification by MS/MS of the identity of peaks for Glc*N*Ac-Mur*N*AcAnh and Glc*N*Ac-Mur*N*AcAnh in the MltA-digested PG samples and SddA reactions. (A, B) Chemical structures of Glc*N*Ac-Mur*N*AcAnh and Glc*N*-Mur*N*AcAnh, respectively. **(C)** and **(D)**, verification of the identity of HPLC peaks labelled in Fig. 1G as Glc*N*-Mur*N*AcAnh and Glc*N*Ac-Mur*N*AcAnh, respectively, by MS and MS/MS. MS/MS analysis of peaks from LC-MS analysis from PG digested with MltA resulted in the same fragmentation shown here. **(C)** Verification using MS/MS (bottom) that the peak with m/z 437 (top) corresponds to Glc*N*-Mur*N*AcAnh. Fragmentation of Glc*N*-Mur*N*AcAnh yields Glc*N*(-H_2O)+H^+ (m/z 162), and not Glc*N*Ac(-H_2O)+H^+ (m/z 204), and Mur*N*AcAnh + H^+ (m/z 276). **(D)** Verification using MS/MS (bottom) that peak with m/z 479 (top) corresponds to Glc*N*Ac-Mur*N*AcAnh. Fragmentation of Glc*N*Ac-Mur*N*AcAnh yields the Glc*N*Ac(-H_2O)+H^+ ion (m/z 204) and MurNAcAnh + H^+ (m/z 276).
(TIF)

S2 Fig. Overexpression of full length SddA in the cytoplasm produces a truncated protein. (A) SDS-PAGE and Western-Blot analysis of soluble (*sol*) and *pellet* fractions from sonicated cell extracts of BL21(DE3) pET28a-HisSddA induced

with IPTG. The His-tag in the N-terminus His-SddA was detected using anti-His-tag antibody. **(B)** AlphaFold model of *E. coli* SddA showing the predicted globular (red) and unfolded C-terminal (grey) regions, plus the location of cleavage sites in His-SddA purified from soluble extracts as the one analysed in A. The identified cleavage sites are P258, V262, K263 and L264.
(TIF)

S3 Fig. SddA is unable to digest peptidoglycan or muropeptides. PG was incubated first with SddA or buffer and then with the muramidase cellosyl (chromatograms labelled "PG") or first with cellosyl and then with SddA or buffer (chromatograms labelled "muropeptides"), to test the activity of SddA on PG or muropeptides, respectively. SddA was added at 10 μM in both cases. SddA treatment did not introduce any changes in the resulting chromatograms.
(TIF)

S4 Fig. SddA can modify denuded glycan strands. (A) Radiolabelled denuded glycan strands were prepared from radiolabelled lipid II ([^{14}C]-lipid II) using transpeptidase-defective PBP1B (S510A), and the amidase AmiC plus its activator NlpD. **(B)** Scheme depicting the preparation of samples (left side) and their analysis (chromatograms on the right side). Muramidase was unable to digest the denuded glycan strands treated with SddA. **(C)** Scheme depicting the preparation of samples (left side) and their analysis (chromatograms on the right side). SddA modified the short oligosaccharides obtained by digesting radiolabelled denuded glycan strands with a muramidase.
(TIF)

S5 Fig. SddA deacetylates Glc*N*Ac residues in denuded glycan strands. (A) Chromatograms of muramidase-digested denuded glycan strands, treated with SddA (red) or buffer (black) after digestion with the muramidase cellosyl. **(B)** Results of MS and MS/MS analysis of the labelled peaks in A. All muropeptide peaks correspond to the non-reduced species.
(TIF)

S6 Fig. *E. coli* SddA contains conserved residues for Zn^{2+} binding. (A) Sequence alignment of *E. coli* SddA with the sequences of the two proteins with a divergent polysaccharide deacetylase domain (PF04748) whose crystal structure is available. These two proteins are BH1492 from *Bacillus halodurans* (PDB 2NLY), which contains a Zn^{2+} in the crystal structure, and ATU2773 from *Agrobacterium tumefaciens* (PDB 2QV5), which does not contain a Zn^{2+} ion in the crystal structure. The sequences are coloured by secondary structure (red indicating alpha helix and blue beta strand). The residues coordinating Zn^{2+} in BH1492 are highlighted in yellow. **(B)** Chromatograms of the analysis of denuded glycan strands treated first with buffer, SddA, SddA$^{24\text{-}238}$, SddA$^{24\text{-}238}$ H78A, or SddA$^{24\text{-}238}$ H123A, and then with the lytic transglycosylase MltA to produce anhydro-muropeptides. Chromatograms for assays with H78A and H123A SddA variants show no Glc*N*-MurAcAnh peak, indicating they are inactive.
(TIF)

S7 Fig. Deletion of *sddA* does not cause morphological changes when growing in LB. (A) BW25113 or BW25513 Δ*ssdA*::kan were grown in LB at 37°C. Samples were collected (arrows), fixed, stained with FM5–95 (cell membrane), immobilized and imaged by phase contrast and epifluorescence microscopy. Representative images are shown. Scale bar is 10 μm. **(B)** morphological measurements and growth doubling time of the cells and growth curves shown in A.
(TIF)

S8 Fig. Deletion of *actS*, *nlpD* or *envC* does not affect OM permeability of cells lacking SddA. (A) Overnight cultures of BW25113 and isogenic Δ*sddA,* Δ*envC,* Δ*actS,* Δ*envC* Δ*sddA,* Δ*actS* Δ*sddA* mutants and **(B)** of BW25113 Δ*nlpD* and isogenic Δ*nlpD* Δ*sddA* were serially diluted and spotted on LB with 5% NaCl plates containing vancomycin (Van), rifampicin (Rif), novobiocin (Nov), mecillinam (Mec), cefsulodin (Cefs), bacitracin (Bac) or SDS/EDTA at the indicated concentrations. Plates were incubated at 37°C for 24 h.
(TIF)

S9 Fig. Deletion of *sddA* increases the sick phenotype of Δ*envC* Δ*nlpD*. BW25113 Δ*envC* Δ*nlpD* and BW25113 Δ*envC* Δ*nlpD* Δ*sddA* were grown in LB at 37°C. At indicated times, samples were taken and imaged on agarose pads containing FM5–95 membrane stain. All scale bars represent 10 μM.
(TIF)

S10 Fig. Co-expression of SddA and EnvC from different plasmids does not rescue OM defects and cell chaining. (A) Overnight cultures of BW25113 harbouring empty pGS100 or pBAD24 plasmids (-/-) or pGS100 with *sddA* (*sddA*/-) or pBAD24 with *envC* (-/*envC*) or both (*ssdA*/*envC*) were serially diluted and spotted onto LB-Lennox supplemented with 25 μg ml^{-1} chloramphenicol and 100 μg ml^{-1} ampicillin containing vancomycin (Van), bacitracin (Bac) or SDS/EDTA at the indicated concentrations. 0.2% arabinose and 0.5 mM IPTG were used to induce *envC* and *sddA* expression, respectively. **(B)** BW25113 cells harbouring pGS100 and pBAD24 or pBAD24 with *envC* (pGS100/*envC*), pGS100 with sddA (*sddA*/pBAD24) or both (*ssdA*/*envC*) were grown in LB with 5% NaCl supplemented with 25 μg ml^{-1} chloramphenicol and 100 μg ml^{-1} ampicillin. IPTG (0.5 mM) and arabinose (0.2%) were used to induce the expression of *sddA* and *envC*, respectively. Samples were collected at the exponential growth phase (arrows) stained with FM5–95 (red, cell membrane) and DAPI (blue, nucleoid), immobilized and imaged by confocal fluorescence microscopy. Representative images are shown. Scale bar is 5 μm.
(TIF)

S11 Fig. Co-expression of SddA and NlpD does not rescue OM defects and cell chaining. (A) Overnight cultures of BW25113 harbouring empty pGS100 or pBAD24 plasmids (-/-) or pGS100 with *sddA* (*sddA*/-) or pBAD24 with *nlpD* (-/*nlpD*) or both (*ssdA*/*nlpD*) were serially diluted and spotted onto LB-Lennox supplemented with 25 μg ml^{-1} chloramphenicol and 100 μg ml^{-1} ampicillin containing vancomycin (Van), bacitracin (Bac) or SDS/EDTA at the indicated concentrations. 0.2% arabinose and 0.5 mM IPTG were used to induce *nlpD* and *sddA* expression, respectively. **(B)** BW25113 cells harbouring pGS100 and pBAD24 or pBAD24 with *nlpD* (pGS100/*nlpD*), pGS100 with sddA (*sddA*/pBAD24) or both (*ssdA*/*nlpD*) were grown in LB-Lennox supplemented with 25 μg ml^{-1} chloramphenicol and 100 μg ml^{-1} ampicillin. IPTG (0.5 mM) and arabinose (0.2%) were used to induce the expression of *sddA* and *nlpD*, respectively. Samples were collected at the exponential growth phase (arrows) stained with FM5–95 (red, cell membrane) and DAPI (blue, nucleoid), immobilized and imaged by confocal fluorescence microscopy. Representative images are shown. Scale bar is 5 μm.
(TIF)

S12 Fig. SddA is expressed at lower levels from the operon with *envC* (A) BW25113 cells harbouring pGS100 or pGS100 encoding *FLAG-sddA* (*sddA*), *FLAG*-sddA H123A (*sddA**) or *envC*/*FLAG-sddA* (*envC*/*sddA*) were grown in LB supplemented with 25 μg ml^{-1} chloramphenicol. 0.5 mM IPTG was added at an OD600 of 0.1, and sample for microscopy were taken when indicated in the growth curves. Cells were imaged using phase contrast. Scale bar is 10 μm. **(B)** BW25113 cells harbouring the same plasmids as described in **(A)** and grown in the same conditions, were harvested after 140 min incubation with 0.5 mM IPTG and FLAG-SddA levels were analysed by Western blot using α-FLAG antibody (right) and SDS-PAGE followed by Coomassie staining was used as loading control (left). Two specific bands were detected labelled as FL (full length) and D (digested). **(C)** Quantification of FLAG-SddA FL and D bands in Western blots as shown in **(B)**, normalized using the Coomassie-stained SDS-PAGE. Values are average ± SD of two repeats, * p-value < 0.05 and n.s. not significant.
(TIF)

S13 Fig. Cell chaining phenotype caused by SddA overproduction is independent of EnvC or FtsX. (A) BW25113 (WT) and BW25113 Δ*envC* (Δ*envC*) cells harbouring pGS100 (ev) or pGS100 expressing *sddA* (SddA) were grown at 37°C in LB with 20 μg ml^{-1} chloramphenicol and expression was induced with 0.5 mM IPTG for 140 min. Samples were imaged by phase contrast and fluorescence microscopy (FM5–95). **(B)** BW25113 (WT) and BW25113 Δ*ftsX* (Δ*ftsX*) cells harbouring pGS100 (ev) or pGS100 expressing *sddA* (SddA) were grown at 30°C in LB with 20 μg ml^{-1} chloramphenicol

supplemented with 0.2 M sucrose and expression was induced with 0.5 mM IPTG for 230 min. Samples were imaged by phase contrast and fluorescence microscopy (FM5–95). Representative images are shown. Scale bar is 5 μm.
(TIF)

S14 Fig. High *sddA* expression in mutants defective in amidase activation aggravates their cell chaining phenotype. (A) Δ*amiC* Δ*nlpD* and Δ*amiB* Δ*amiA* Δ*envC* cells harbouring pGS100 or pGS100 expressing *sddA* were grown in LB with 5% NaCl supplemented with chloramphenicol at 25 μg ml^{-1}. Samples were collected (arrows) stained with FM5–95 (red, cell membrane) and DAPI (blue, nucleoid), immobilized and imaged by confocal fluorescence microscopy. Representative images are shown. Scale bar is 5 μm. **(B)** Doubling time of cultures shown in panel A.
(TIF)

S15 Fig. SddA-sfGFP overproduction causes chaining in an IPTG-dependent manner. (A) BW25113 cells harbouring pGS100 (ev) or pGS100 expressing *sddA*, *sddA::sfgfp* (WT) or *sddA D179A::sfgfp* (D179A) were grown in LB with 20 μg ml^{-1} chloramphenicol at 37°C and expression of the fluorescent constructs was induced with 0.5 mM IPTG for 140 min. Samples were pelleted, protein extracts were obtained by sonication and quantified by BCA. 15 μg of each extract was loaded per lane, separated by SDS-PAGE and GFP was immunodetected by Western blot using α-GFP antibody. (*, unspecific bands) (**B**) BW25113 cells harbouring pGS100 (ev) or pGS100 encoding *sddA::sfGFP* (SddA) were grown in LB with 20 μg ml^{-1} chloramphenicol at 37°C and expression of the fluorescent construct was induced with the indicated amount of IPTG for 140 min. For ev, samples cell membranes were stained with FM5–95 dye. Samples were imaged by phase contrast (PC) and fluorescence microscopy (GFP or FM5–95). Representative images are shown. Scale bar is 5 μm.
(TIF)

S16 Fig. Alphafold-predicted interaction between SddA and EnvC or SddA and FtsX. Best models obtained by Alphafold of hypothetical SddA-EnvC, **(A)**, and SddA-FtsX complexes, **(B)**; and their corresponding Predicted Aligned Error (PAE) matrices **(C)** and **(D)**, respectively. Each cell in the PAE matrices represents the estimate alignment error (in Å) between pairs of residues across the predicted protein structure, with darker shades indicating lower PAE and higher model confidence.
(TIF)

S17 Fig. SddA D179A is active against denuded strands. Chromatograms of the analysis of denuded glycan strands treated first with buffer, His-$SddA^{24-238}$ or His-$SddA^{24-238}$ D179A, and then with the lytic transglycosylase MltA. MltA fully digested denuded strands producing anhydro sugars. Reactions contained 2 μM of enzyme and were incubated at 37°C for 24 h. Peak labelled Glc*N* corresponds to Glc*N*-Mur*N*AcAnh and peak labelled Glc*N*Ac corresponds to Glc*N*Ac-Mur*N*AcAnh.
(TIF)

S18 Fig. The mutation D179A induces localized and global changes in SddA dynamics, particularly in regions critical for binding to EnvC. Residue-resolved root mean square fluctuations (RMSF) of wild-type (WT, green) and D179A mutant (red) SddA, calculated from molecular dynamics simulations. The blue curve represents the difference in fluctuations (ΔRMSF) between WT and mutant (WT - mutant). Negative ΔRMSF values indicate greater rigidity in the mutant, while positive values reflect increased flexibility. Residues involved in interaction with EnvC, as predicted by AlphaFold, are highlighted in the analysis.
(TIF)

S19 Fig. SddA does not significantly inhibit ActS-AmiC or EnvC-AmiA. (A, B) HPLC-based end-point activity assays for EnvC-AmiA or ActS-AmiC amidase-activator pairs, in the presence or absence of $SddA^{24-238}$. Sacculi from *E. coli*

BW25113Δ6LDT were incubated with 2 μM of the indicated amidase and activator, in the presence or absence of 4 μM His-SddA$^{24-238}$ (SddA$^{24-238}$). EnvC(fl) indicates the EnvC construct containing the LytM and coiled-coiled domain whereas EnvC(LytM) indicates the construct with only the LytM domain. Reactions were incubated for 2 h **(A)** or 1 h **(B)** at 37°C. Representative chromatograms are shown. **(C)** Chromatograms for the control reactions showing no activation of AmiA or AmiC by SddA$^{24-238}$. Reactions contained 2 μM of each protein and *E. coli* MC1061 PG and were incubated for 2 h at 37°C. **(D)** Quantification of muropeptides peak areas (peaks 4, 5 and 6) in reactions depicted in A and B, normalized against the areas of those peaks in the controls with no enzyme. Values are average + /- variation of 2 reactions. There was a slight activation of EnvC(LytM)-AmiA activity by SddA. **(E)** Identity and structures of the peaks labelled in A-C and Fig 6A. G stands for Glc*N*Ac, M for Mur*N*AcAnh and G' for Glc*N*.
(TIF)

S1 Table. Strains used in this work.
(DOCX)

S2 Table. Plasmids used in this work.
(DOCX)

S3 Table. Oligonucleotides used in this work.
(DOCX)

S4 Table. Raw data for Figs 2C, 2E, 7B, S7B, S12C, and S19D.
(XLSX)

Author contributions

Conceptualization: Víctor M. Hernández-Rocamora, Alessandra M. Martorana, Amilcar J. Perez, Jie Xiao, Manuel Pazos, Alessandra Polissi, Waldemar Vollmer.

Data curation: Víctor M. Hernández-Rocamora, Bogdan I. Iorga.

Formal analysis: Víctor M. Hernández-Rocamora, Alessandra M. Martorana, Aitana Belloso, Daniel Ballesteros, Marta Zaccaria, Amilcar J. Perez, Bogdan I. Iorga, David Abia, Joe Gray, Jie Xiao, Manuel Pazos, Alessandra Polissi, Waldemar Vollmer.

Funding acquisition: Alessandra M. Martorana, Jie Xiao, Manuel Pazos, Waldemar Vollmer.

Investigation: Víctor M. Hernández-Rocamora, Aitana Belloso, Daniel Ballesteros, Marta Zaccaria, Bogdan I. Iorga, David Abia, Joe Gray.

Methodology: Víctor M. Hernández-Rocamora, Waldemar Vollmer.

Resources: Eefjan Breukink.

Supervision: Alessandra M. Martorana, Waldemar Vollmer.

Validation: Alessandra M. Martorana.

Writing – original draft: Víctor M. Hernández-Rocamora, Alessandra M. Martorana, Aitana Belloso, Daniel Ballesteros, Marta Zaccaria, Amilcar J. Perez, Bogdan I. Iorga, David Abia, Joe Gray, Jie Xiao, Manuel Pazos, Alessandra Polissi, Waldemar Vollmer.

Writing – review & editing: Víctor M. Hernández-Rocamora, Alessandra M. Martorana, Aitana Belloso, Daniel Ballesteros, Marta Zaccaria, Amilcar J. Perez, Bogdan I. Iorga, David Abia, Joe Gray, Jie Xiao, Manuel Pazos, Alessandra Polissi, Waldemar Vollmer.

References

1. Vollmer W, Blanot D, de Pedro MA. Peptidoglycan structure and architecture. FEMS Microbiol Rev. 2008;32(2):149–67. https://doi.org/10.1111/j.1574-6976.2007.00094.x PMID: 18194336
2. Egan AJF, Errington J, Vollmer W. Regulation of peptidoglycan synthesis and remodelling. Nat Rev Microbiol. 2020;18(8):446–60. https://doi.org/10.1038/s41579-020-0366-3 PMID: 32424210
3. Typas A, Banzhaf M, Gross CA, Vollmer W. From the regulation of peptidoglycan synthesis to bacterial growth and morphology. Nat Rev Microbiol. 2011;10(2):123–36. https://doi.org/10.1038/nrmicro2677 PMID: 22203377
4. Gray AN, Egan AJF, Van't Veer IL, Verheul J, Colavin A, Koumoutsi A, et al. Coordination of peptidoglycan synthesis and outer membrane constriction during Escherichia coli cell division. Elife. 2015;4:e07118. https://doi.org/10.7554/eLife.07118 PMID: 25951518
5. Mamou G, Corona F, Cohen-Khait R, Housden NG, Yeung V, Sun D, et al. Peptidoglycan maturation controls outer membrane protein assembly. Nature. 2022;606(7916):953–9. https://doi.org/10.1038/s41586-022-04834-7 PMID: 35705811
6. Bisson-Filho AW, Hsu Y-P, Squyres GR, Kuru E, Wu F, Jukes C, et al. Treadmilling by FtsZ filaments drives peptidoglycan synthesis and bacterial cell division. Science. 2017;355(6326):739–43. https://doi.org/10.1126/science.aak9973 PMID: 28209898
7. Yang X, Lyu Z, Miguel A, McQuillen R, Huang KC, Xiao J. GTPase activity-coupled treadmilling of the bacterial tubulin FtsZ organizes septal cell wall synthesis. Science. 2017;355(6326):744–7. https://doi.org/10.1126/science.aak9995 PMID: 28209899
8. Monteiro JM, Pereira AR, Reichmann NT, Saraiva BM, Fernandes PB, Veiga H, et al. Peptidoglycan synthesis drives an FtsZ-treadmilling-independent step of cytokinesis. Nature. 2018;554(7693):528–32. https://doi.org/10.1038/nature25506 PMID: 29443967
9. Mahone CR, Goley ED. Bacterial cell division at a glance. J Cell Sci. 2020;133(7):jcs237057. https://doi.org/10.1242/jcs.237057 PMID: 32269092
10. Pazos M, Vollmer W. Regulation and function of class A Penicillin-binding proteins. Curr Opin Microbiol. 2021;60:80–7. https://doi.org/10.1016/j.mib.2021.01.008 PMID: 33611146
11. Pazos M, Peters K, Casanova M, Palacios P, VanNieuwenhze M, Breukink E, et al. Z-ring membrane anchors associate with cell wall synthases to initiate bacterial cell division. Nat Commun. 2018;9(1):5090. https://doi.org/10.1038/s41467-018-07559-2 PMID: 30504892
12. Pazos M, Peters K, Boes A, Safaei Y, Kenward C, Caveney NA, et al. SPOR Proteins Are Required for Functionality of Class A Penicillin-Binding Proteins in Escherichia coli. mBio. 2020;11(6):e02796-20. https://doi.org/10.1128/mBio.02796-20 PMID: 33144379
13. Pazos M, Peters K, Vollmer W. Robust peptidoglycan growth by dynamic and variable multi-protein complexes. Curr Opin Microbiol. 2017;36:55–61. https://doi.org/10.1016/j.mib.2017.01.006 PMID: 28214390
14. Heidrich C, Templin MF, Ursinus A, Merdanovic M, Berger J, Schwarz H, et al. Involvement of N-acetylmuramyl-L-alanine amidases in cell separation and antibiotic-induced autolysis of *Escherichia coli*. Mol Microbiol. 2001;41(1):167–78. https://doi.org/10.1046/j.1365-2958.2001.02499.x PMID: 11454209
15. Priyadarshini R, de Pedro MA, Young KD. Role of peptidoglycan amidases in the development and morphology of the division septum in *Escherichia coli*. J Bacteriol. 2007;189(14):5334–47. https://doi.org/10.1128/JB.00415-07 PMID: 17483214
16. Uehara T, Dinh T, Bernhardt TG. LytM-domain factors are required for daughter cell separation and rapid ampicillin-induced lysis in Escherichia coli. J Bacteriol. 2009;191(16):5094–107. https://doi.org/10.1128/JB.00505-09 PMID: 19525345
17. Chen Y, Gu J, Yang B, Yang L, Pang J, Luo Q, et al. Structure and activity of the septal peptidoglycan hydrolysis machinery crucial for bacterial cell division. PLoS Biol. 2024;22(5):e3002628. https://doi.org/10.1371/journal.pbio.3002628 PMID: 38814940
18. Hao A, Suo Y, Lee S-Y. Structural insights into the FtsEX-EnvC complex regulation on septal peptidoglycan hydrolysis in Vibrio cholerae. Structure. 2024;32(2):188-199.e5. https://doi.org/10.1016/j.str.2023.11.007 PMID: 38070498
19. Xu X, Li J, Chua W-Z, Pages MA, Shi J, Hermoso JA, et al. Mechanistic insights into the regulation of cell wall hydrolysis by FtsEX and EnvC at the bacterial division site. Proc Natl Acad Sci U S A. 2023;120(21):e2301897120. https://doi.org/10.1073/pnas.2301897120 PMID: 37186861
20. Cook J, Baverstock TC, McAndrew MBL, Roper DI, Stansfeld PJ, Crow A. Activator-induced conformational changes regulate division-associated peptidoglycan amidases. Proc Natl Acad Sci U S A. 2023;120(24). https://doi.org/10.1073/pnas.2302580120 PMID: 37276423
21. Gurnani Serrano CK, Winkle M, Martorana AM, Biboy J, Morè N, Moynihan P, et al. ActS activates peptidoglycan amidases during outer membrane stress in Escherichia coli. Mol Microbiol. 2021;116(1):329–42. https://doi.org/10.1111/mmi.14712 PMID: 33660879
22. Mueller EA, Iken AG, Ali Öztürk M, Winkle M, Schmitz M, Vollmer W, et al. The active repertoire of *Escherichia coli* peptidoglycan amidases varies with physiochemical environment. Mol Microbiol. 2021;116(1):311–28. https://doi.org/10.1111/mmi.14711 PMID: 33666292
23. Tsang M-J, Yakhnina AA, Bernhardt TG. NlpD links cell wall remodeling and outer membrane invagination during cytokinesis in *Escherichia coli*. PLoS Genet. 2017;13(7):e1006888. https://doi.org/10.1371/journal.pgen.1006888 PMID: 28708841
24. Boelter G, Bryant JA, Doherty H, Wotherspoon P, Alodaini D, Ma X, et al. The lipoprotein DolP affects cell separation in Escherichia coli, but not as an upstream regulator of NlpD. Microbiology (Reading). 2022;168(5). https://doi.org/10.1099/mic.0.001197 PMID: 35604759
25. Szczepaniak J, Press C, Kleanthous C. The multifarious roles of Tol-Pal in Gram-negative bacteria. FEMS Microbiol Rev. 2020;44(4):490–506. https://doi.org/10.1093/femsre/fuaa018 PMID: 32472934
26. Vollmer W. Structural variation in the glycan strands of bacterial peptidoglycan. FEMS Microbiol Rev. 2008;32(2):287–306. https://doi.org/10.1111/j.1574-6976.2007.00088.x PMID: 18070068

27. Vollmer W, Tomasz A. The pgdA gene encodes for a peptidoglycan N-acetylglucosamine deacetylase in Streptococcus pneumoniae. J Biol Chem. 2000;275(27):20496–501. https://doi.org/10.1074/jbc.M910189199 PMID: 10781617
28. Vollmer W, Tomasz A. Peptidoglycan N-acetylglucosamine deacetylase, a putative virulence factor in *Streptococcus pneumoniae*. Infect Immun. 2002;70(12):7176–8. https://doi.org/10.1128/IAI.70.12.7176-7178.2002 PMID: 12438406
29. Boneca IG, Dussurget O, Cabanes D, Nahori M-A, Sousa S, Lecuit M, et al. A critical role for peptidoglycan N-deacetylation in Listeria evasion from the host innate immune system. Proc Natl Acad Sci U S A. 2007;104(3):997–1002. https://doi.org/10.1073/pnas.0609672104 PMID: 17215377
30. Fittipaldi N, Sekizaki T, Takamatsu D, de la Cruz Domínguez-Punaro M, Harel J, Bui NK, et al. Significant contribution of the pgdA gene to the virulence of Streptococcus suis. Mol Microbiol. 2008;70(5):1120–35. https://doi.org/10.1111/j.1365-2958.2008.06463.x PMID: 18990186
31. Blair DE, Schüttelkopf AW, MacRae JI, van Aalten DMF. Structure and metal-dependent mechanism of peptidoglycan deacetylase, a streptococcal virulence factor. Proc Natl Acad Sci U S A. 2005;102(43):15429–34. https://doi.org/10.1073/pnas.0504339102 PMID: 16221761
32. Wang G, Maier SE, Lo LF, Maier G, Dosi S, Maier RJ. Peptidoglycan deacetylation in Helicobacter pylori contributes to bacterial survival by mitigating host immune responses. Infect Immun. 2010;78(11):4660–6. https://doi.org/10.1128/IAI.00307-10 PMID: 20805339
33. Shaik MM, Cendron L, Percudani R, Zanotti G. The structure of *Helicobacter pylori* HP0310 reveals an atypical peptidoglycan deacetylase. PLoS One. 2011;6(4):e19207. https://doi.org/10.1371/journal.pone.0019207 PMID: 21559431
34. Sycuro LK, Pincus Z, Gutierrez KD, Biboy J, Stern CA, Vollmer W, et al. Peptidoglycan crosslinking relaxation promotes *Helicobacter pylori's* helical shape and stomach colonization. Cell. 2010;141(5):822–33. https://doi.org/10.1016/j.cell.2010.03.046 PMID: 20510929
35. Sycuro LK, Wyckoff TJ, Biboy J, Born P, Pincus Z, Vollmer W, et al. Multiple peptidoglycan modification networks modulate Helicobacter pylori's cell shape, motility, and colonization potential. PLoS Pathog. 2012;8(3):e1002603. https://doi.org/10.1371/journal.ppat.1002603 PMID: 22457625
36. Chaput C, Ecobichon C, Cayet N, Girardin SE, Werts C, Guadagnini S, et al. Role of AmiA in the morphological transition of Helicobacter pylori and in immune escape. PLoS Pathog. 2006;2(9):e97. https://doi.org/10.1371/journal.ppat.0020097 PMID: 17002496
37. Chaput C, Labigne A, Boneca IG. Characterization of *Helicobacter pylori* lytic transglycosylases Slt and MltD. J Bacteriol. 2007;189(2):422–9. https://doi.org/10.1128/JB.01270-06 PMID: 17085576
38. Patel AV, Turner RD, Rifflet A, Acosta-Martin AE, Nichols A, Awad MM, et al. PGFinder, a novel analysis pipeline for the consistent, reproducible, and high-resolution structural analysis of bacterial peptidoglycans. Elife. 2021;10:e70597. https://doi.org/10.7554/eLife.70597 PMID: 34579805
39. Glauner B, Höltje JV, Schwarz U. The composition of the murein of *Escherichia coli*. Journal of Biological Chemistry. 1988;263(21):10088–95. https://doi.org/10.1016/s0021-9258(19)81481-3
40. Glauner B. Separation and quantification of muropeptides with high-performance liquid chromatography. Anal Biochem. 1988;172(2):451–64. https://doi.org/10.1016/0003-2697(88)90468-x PMID: 3056100
41. Itoh Y, Rice JD, Goller C, Pannuri A, Taylor J, Meisner J, et al. Roles of pgaABCD genes in synthesis, modification, and export of the *Escherichia coli* biofilm adhesin poly-beta-1,6-N-acetyl-D-glucosamine. J Bacteriol. 2008;190(10):3670–80. https://doi.org/10.1128/JB.01920-07 PMID: 18359807
42. Wang X, Preston JF 3rd, Romeo T. The pgaABCD locus of *Escherichia coli* promotes the synthesis of a polysaccharide adhesin required for biofilm formation. J Bacteriol. 2004;186(9):2724–34. https://doi.org/10.1128/JB.186.9.2724-2734.2004 PMID: 15090514
43. Hu P, Janga SC, Babu M, Díaz-Mejía JJ, Butland G, Yang W, et al. Global functional atlas of *Escherichia coli* encompassing previously uncharacterized proteins. PLoS Biol. 2009;7(4):e96. https://doi.org/10.1371/journal.pbio.1000096 PMID: 19402753
44. Mendler K, Chen H, Parks DH, Lobb B, Hug LA, Doxey AC. AnnoTree: visualization and exploration of a functionally annotated microbial tree of life. Nucleic Acids Res. 2019;47(9):4442–8. https://doi.org/10.1093/nar/gkz246 PMID: 31081040
45. Ursinus A, Höltje JV. Purification and properties of a membrane-bound lytic transglycosylase from Escherichia coli. J Bacteriol. 1994;176(2):338–43. https://doi.org/10.1128/jb.176.2.338-343.1994 PMID: 8288527
46. Lommatzsch J, Templin MF, Kraft AR, Vollmer W, Höltje JV. Outer membrane localization of murein hydrolases: MltA, a third lipoprotein lytic transglycosylase in Escherichia coli. J Bacteriol. 1997;179(17):5465–70. https://doi.org/10.1128/jb.179.17.5465-5470.1997 PMID: 9287002
47. Yahashiri A, Jorgenson MA, Weiss DS. Bacterial SPOR domains are recruited to septal peptidoglycan by binding to glycan strands that lack stem peptides. Proc Natl Acad Sci U S A. 2015;112(36):11347–52. https://doi.org/10.1073/pnas.1508536112 PMID: 26305949
48. Ursinus A, van den Ent F, Brechtel S, de Pedro M, Höltje J-V, Löwe J, et al. Murein (peptidoglycan) binding property of the essential cell division protein FtsN from Escherichia coli. J Bacteriol. 2004;186(20):6728–37. https://doi.org/10.1128/JB.186.20.6728-6737.2004 PMID: 15466024
49. Yahashiri A, Jorgenson MA, Weiss DS. The SPOR Domain, a Widely Conserved Peptidoglycan Binding Domain That Targets Proteins to the Site of Cell Division. J Bacteriol. 2017;199(14):e00118-17. https://doi.org/10.1128/JB.00118-17 PMID: 28396350
50. Müller P, Ewers C, Bertsche U, Anstett M, Kallis T, Breukink E, et al. The essential cell division protein FtsN interacts with the murein (peptidoglycan) synthase PBP1B in Escherichia coli. J Biol Chem. 2007;282(50):36394–402. https://doi.org/10.1074/jbc.M706390200 PMID: 17938168
51. Arends SJR, Williams K, Scott RJ, Rolong S, Popham DL, Weiss DS. Discovery and characterization of three new *Escherichia coli* septal ring proteins that contain a SPOR domain: DamX, DedD, and RlpA. J Bacteriol. 2010;192(1):242–55. https://doi.org/10.1128/JB.01244-09 PMID: 19880599
52. Heidrich C, Ursinus A, Berger J, Schwarz H, Höltje J-V. Effects of multiple deletions of murein hydrolases on viability, septum cleavage, and sensitivity to large toxic molecules in *Escherichia coli*. J Bacteriol. 2002;184(22):6093–9. https://doi.org/10.1128/JB.184.22.6093-6099.2002 PMID: 12399477

53. Georgopapadakou NH, Smith SA, Sykes RB. Mode of action of azthreonam. Antimicrob Agents Chemother. 1982;21(6):950–6. https://doi.org/10.1128/AAC.21.6.950 PMID: 6180685

54. de Pedro MA, Quintela JC, Höltje JV, Schwarz H. Murein segregation in *Escherichia coli*. J Bacteriol. 1997;179(9):2823–34. https://doi.org/10.1128/jb.179.9.2823-2834.1997 PMID: 9139895

55. Yakhnina AA, Bernhardt TG. The Tol-Pal system is required for peptidoglycan-cleaving enzymes to complete bacterial cell division. Proc Natl Acad Sci U S A. 2020;117(12):6777–83. https://doi.org/10.1073/pnas.1919267117 PMID: 32152098

56. Cascales E, Lloubès R, Sturgis JN. The TolQ-TolR proteins energize TolA and share homologies with the flagellar motor proteins MotA-MotB. Mol Microbiol. 2001;42(3):795–807. https://doi.org/10.1046/j.1365-2958.2001.02673.x PMID: 11722743

57. Uehara T, Parzych KR, Dinh T, Bernhardt TG. Daughter cell separation is controlled by cytokinetic ring-activated cell wall hydrolysis. EMBO J. 2010;29(8):1412–22. https://doi.org/10.1038/emboj.2010.36 PMID: 20300061

58. Kaus GM, Snyder LF, Müh U, Flores MJ, Popham DL, Ellermeier CD. Lysozyme Resistance in Clostridioides difficile Is Dependent on Two Peptidoglycan Deacetylases. J Bacteriol. 2020;202(22):e00421-20. https://doi.org/10.1128/JB.00421-20 PMID: 32868404

59. Dobihal GS, Flores-Kim J, Roney IJ, Wang X, Rudner DZ. The WalR-WalK Signaling Pathway Modulates the Activities of both CwlO and LytE through Control of the Peptidoglycan Deacetylase PdaC in *Bacillus subtilis*. J Bacteriol. 2022;204(2):e0053321. https://doi.org/10.1128/JB.00533-21 PMID: 34871030

60. Arnaouteli S, Giastas P, Andreou A, Tzanodaskalaki M, Aldridge C, Tzartos SJ, et al. Two Putative Polysaccharide Deacetylases Are Required for Osmotic Stability and Cell Shape Maintenance in *Bacillus anthracis*. J Biol Chem. 2015;290(21):13465–78. https://doi.org/10.1074/jbc.M115.640029 PMID: 25825488

61. Coullon H, Rifflet A, Wheeler R, Janoir C, Boneca IG, Candela T. N-Deacetylases required for muramic-δ-lactam production are involved in *Clostridium difficile* sporulation, germination, and heat resistance. J Biol Chem. 2018;293(47):18040–54. https://doi.org/10.1074/jbc.RA118.004273 PMID: 30266804

62. Benachour A, Ladjouzi R, Le Jeune A, Hébert L, Thorpe S, Courtin P, et al. The lysozyme-induced peptidoglycan N-acetylglucosamine deacetylase PgdA (EF1843) is required for *Enterococcus faecalis* virulence. J Bacteriol. 2012;194(22):6066–73. https://doi.org/10.1128/JB.00981-12 PMID: 22961856

63. Huber M, Faure G, Laass S, Kolbe E, Seitz K, Wehrheim C, et al. Translational coupling via termination-reinitiation in archaea and bacteria. Nat Commun. 2019;10(1):4006. https://doi.org/10.1038/s41467-019-11999-9 PMID: 31488843

64. Corbin Goodman LC, Erickson HP. FtsZ at mid-cell is essential in *Escherichia coli* until the late stage of constriction. Microbiology (Reading). 2022;168(6). https://doi.org/10.1099/mic.0.001194 PMID: 35679326

65. Silber N, Mayer C, Matos de Opitz CL, Sass P. Progression of the late-stage divisome is unaffected by the depletion of the cytoplasmic FtsZ pool. Commun Biol. 2021;4(1):270. https://doi.org/10.1038/s42003-021-01789-9 PMID: 33649500

66. Baba T, Ara T, Hasegawa M, Takai Y, Okumura Y, Baba M, et al. Construction of *Escherichia coli* K-12 in-frame, single-gene knockout mutants: the Keio collection. Mol Syst Biol. 2006;2. https://doi.org/10.1038/msb4100050 PMID: 16738554

67. Datsenko KA, Wanner BL. One-step inactivation of chromosomal genes in *Escherichia coli K-12* using PCR products. Proc Natl Acad Sci U S A. 2000;97(12):6640–5. https://doi.org/10.1073/pnas.120163297 PMID: 10829079

68. Seco EM, Fernandez LA. Efficient markerless integration of genes in the chromosome of probiotic *E. coli* Nissle 1917 by bacterial conjugation. Microb Biotechnol. 2022;15(5):1374–91. Epub 20211109. https://doi.org/10.1111/1751-7915.13967 PMID: 34755474; PMCID: PMC9049610.

69. Reddy M. Role of FtsEX in cell division of *Escherichia coli*: viability of ftsEX mutants is dependent on functional SufI or high osmotic strength. J Bacteriol. 2007;189(1):98–108. https://doi.org/10.1128/JB.01347-06 PMID: 17071757

70. Silhavy TJ, Berman ML, Enquist LW, Laboratory CSH. Experiments with gene fusions: Cold Spring Harbor Laboratory; 1984.

71. Pennartz A, Généreux C, Parquet C, Mengin-Lecreulx D, Joris B. Substrate-induced inactivation of the *Escherichia coli* AmiD N-acetylmuramoyl-L-alanine amidase highlights a new strategy to inhibit this class of enzyme. Antimicrob Agents Chemother. 2009;53(7):2991–7. https://doi.org/10.1128/AAC.01520-07 PMID: 19237650

72. Van Straaten KE, Dijkstra BW, Thunnissen AMWH. Purification, crystallization and preliminary X-ray analysis of the lytic transglycosylase MltA from *Escherichia coli*. Acta Crystallogr D Biol Crystallogr. 2004;60(Pt 4):758–60. https://doi.org/10.1107/S0907444904002574 PMID: 15039577

73. Bertsche U, Kast T, Wolf B, Fraipont C, Aarsman MEG, Kannenberg K, et al. Interaction between two murein (peptidoglycan) synthases, PBP3 and PBP1B, in *Escherichia coli*. Mol Microbiol. 2006;61(3):675–90. https://doi.org/10.1111/j.1365-2958.2006.05280.x PMID: 16803586

74. Egan AJF, Jean NL, Koumoutsi A, Bougault CM, Biboy J, Sassine J, et al. Outer-membrane lipoprotein LpoB spans the periplasm to stimulate the peptidoglycan synthase PBP1B. Proc Natl Acad Sci U S A. 2014;111(22):8197–202. https://doi.org/10.1073/pnas.1400376111 PMID: 24821816

75. Breukink E, van Heusden HE, Vollmerhaus PJ, Swiezewska E, Brunner L, Walker S, et al. Lipid II is an intrinsic component of the pore induced by nisin in bacterial membranes. J Biol Chem. 2003;278(22):19898–903. https://doi.org/10.1074/jbc.M301463200 PMID: 12663672

76. Bertsche U, Breukink E, Kast T, Vollmer W. In vitro murein peptidoglycan synthesis by dimers of the bifunctional transglycosylase-transpeptidase PBP1B from *Escherichia coli*. J Biol Chem. 2005;280(45):38096–101. https://doi.org/10.1074/jbc.M508646200 PMID: 16154998

77. Biboy J, Bui NK, Vollmer W. *In vitro* peptidoglycan synthesis assay with lipid II substrate. In: Delcour AH, Editor. Bacterial Cell Surfaces: Methods and Protocols. Totowa, NJ: Humana Press; 2013. p. 273–88.

78. Cutler KJ, Stringer C, Lo TW, Rappez L, Stroustrup N, Brook Peterson S, et al. Omnipose: a high-precision morphology-independent solution for bacterial cell segmentation. Nat Methods. 2022;19(11):1438–48. https://doi.org/10.1038/s41592-022-01639-4 PMID: 36253643

79. Morè N, Martorana AM, Biboy J, Otten C, Winkle M, Serrano CKG, et al. Peptidoglycan Remodeling Enables *Escherichia coli* To Survive Severe Outer Membrane Assembly Defect. mBio. 2019;10(1):e02729-18. https://doi.org/10.1128/mBio.02729-18 PMID: 30723128

80. Lyu Z, Yahashiri A, Yang X, McCausland JW, Kaus GM, McQuillen R, et al. FtsN maintains active septal cell wall synthesis by forming a processive complex with the septum-specific peptidoglycan synthases in *E. coli*. Nat Commun. 2022;13(1):5751. https://doi.org/10.1038/s41467-022-33404-8 PMID: 36180460

81. Neidhardt FC, Bloch PL, Smith DF. Culture medium for enterobacteria. J Bacteriol. 1974;119(3):736–47. https://doi.org/10.1128/jb.119.3.736-747.1974 PMID: 4604283

82. Letunic I, Bork P. Interactive Tree of Life (iTOL) v6: recent updates to the phylogenetic tree display and annotation tool. Nucleic Acids Res. 2024;52(W1):W78–82. https://doi.org/10.1093/nar/gkae268 PMID: 38613393

83. Jumper J, Evans R, Pritzel A, Green T, Figurnov M, Ronneberger O, et al. Highly accurate protein structure prediction with AlphaFold. Nature. 2021;596(7873):583–9. https://doi.org/10.1038/s41586-021-03819-2 PMID: 34265844

84. Evans R, O'Neill M, Pritzel A, Antropova N, Senior A, Green T, et al. Protein complex prediction with AlphaFold-Multimer. bioRxiv. 2022. doi: 10.1101/2021.10.04.463034

85. Berman HM, Westbrook J, Feng Z, Gilliland G, Bhat TN, Weissig H, et al. The Protein Data Bank. Nucleic Acids Res. 2000;28(1):235–42. https://doi.org/10.1093/nar/28.1.235 PMID: 10592235

86. Gordon JC, Myers JB, Folta T, Shoja V, Heath LS, Onufriev A. H++: a server for estimating pKas and adding missing hydrogens to macromolecules. Nucleic Acids Res. 2005;33(Web Server issue):W368-71. https://doi.org/10.1093/nar/gki464 PMID: 15980491

87. Case DA, Aktulga HM, Belfon K, Cerutti DS, Cisneros GA, Cruzeiro VWD, et al. AmberTools. J Chem Inf Model. 2023;63(20):6183–91. https://doi.org/10.1021/acs.jcim.3c01153 PMID: 37805934

88. Tian C, Kasavajhala K, Belfon KAA, Raguette L, Huang H, Migues AN, et al. ff19SB: Amino-Acid-Specific Protein Backbone Parameters Trained against Quantum Mechanics Energy Surfaces in Solution. J Chem Theory Comput. 2020;16(1):528–52. https://doi.org/10.1021/acs.jctc.9b00591 PMID: 31714766

89. Izadi S, Anandakrishnan R, Onufriev AV. Building Water Models: A Different Approach. J Phys Chem Lett. 2014;5(21):3863–71. https://doi.org/10.1021/jz501780a PMID: 25400877

90. Hopkins CW, Le Grand S, Walker RC, Roitberg AE. Long-Time-Step Molecular Dynamics through Hydrogen Mass Repartitioning. J Chem Theory Comput. 2015;11(4):1864–74. https://doi.org/10.1021/ct5010406 PMID: 26574392

91. Shirts MR, Klein C, Swails JM, Yin J, Gilson MK, Mobley DL, et al. Lessons learned from comparing molecular dynamics engines on the SAMPL5 dataset. J Comput Aided Mol Des. 2017;31(1):147–61. https://doi.org/10.1007/s10822-016-9977-1 PMID: 27787702

92. Loncharich RJ, Brooks BR, Pastor RW. Langevin dynamics of peptides: the frictional dependence of isomerization rates of N-acetylalanyl-N'-methylamide. Biopolymers. 1992;32(5):523–35. https://doi.org/10.1002/bip.360320508 PMID: 1515543

93. Åqvist J, Wennerström P, Nervall M, Bjelic S, Brandsdal BO. Molecular dynamics simulations of water and biomolecules with a Monte Carlo constant pressure algorithm. Chemical Physics Letters. 2004;384(4–6):288–94. https://doi.org/10.1016/j.cplett.2003.12.039

94. Darden T, York D, Pedersen L. Particle mesh Ewald: An N·log(N) method for Ewald sums in large systems. The Journal of Chemical Physics. 1993;98(12):10089–92. https://doi.org/10.1063/1.464397

95. Roe DR, Cheatham TE 3rd. PTRAJ and CPPTRAJ: Software for Processing and Analysis of Molecular Dynamics Trajectory Data. J Chem Theory Comput. 2013;9(7):3084–95. https://doi.org/10.1021/ct400341p PMID: 26583988